

Young Dentate Granule Cells Mediate Pattern Separation, whereas Old Granule Cells Facilitate Pattern Completion

Toshiaki Nakashiba,¹ Jesse D. Cushman,² Kenneth A. Pelkey,³ Sophie Renaudineau,¹ Derek L. Buhl,¹ Thomas J. McHugh,^{1,5} Vanessa Rodriguez Barrera,² Ramesh Chittajallu,³ Keisuke S. Iwamoto,⁴ Chris J. McBain,³ Michael S. Fanselow,² and Susumu Tonegawa^{1,*}

¹Departments of Biology and Brain and Cognitive Sciences, RIKEN-MIT Center for Neural Circuit Genetics at The Picower Institute for Learning and Memory, Massachusetts Institute of Technology, Cambridge, MA 02139, USA

²Department of Psychology, Department of Psychiatry and Biobehavioral Sciences, University of California, Los Angeles, Los Angeles, CA 90095, USA

³Laboratory of Cellular and Synaptic Neurophysiology, Eunice Kennedy Shriver National Institute of Child Health and Human Development, National Institutes of Health, Bethesda, MD 20892, USA

⁴Department of Radiation Oncology, David Geffen School of Medicine, University of California, Los Angeles, Los Angeles, CA 90095, USA

⁵Present address: RIKEN Brain Science Institute, 2-1 Hirosawa, Wako-Shi, Saitama 351-0198, Japan

*Correspondence: tonegawa@mit.edu

DOI 10.1016/j.cell.2012.01.046

SUMMARY

Adult-born granule cells (GCs), a minor population of cells in the hippocampal dentate gyrus, are highly active during the first few weeks after functional integration into the neuronal network, distinguishing them from less active, older adult-born GCs and the major population of dentate GCs generated developmentally. To ascertain whether young and old GCs perform distinct memory functions, we created a transgenic mouse in which output of old GCs was specifically inhibited while leaving a substantial portion of young GCs intact. These mice exhibited enhanced or normal pattern separation between similar contexts, which was reduced following ablation of young GCs. Furthermore, these mutant mice exhibited deficits in rapid pattern completion. Therefore, pattern separation requires adult-born young GCs but not old GCs, and older GCs contribute to the rapid recall by pattern completion. Our data suggest that as adult-born GCs age, their function switches from pattern separation to rapid pattern completion.

INTRODUCTION

The hippocampus plays a crucial role in episodic memory (Scoville and Milner, 1957; Burgess et al., 2002; Squire et al., 2004). It allows the formation of distinct memories of similar episodes by generating distinct representations of the temporal and spatial relationships comprising the events (pattern separation). This ability of the hippocampus is critical because many episodes we experience daily have similarities, but it is often important

to memorize distinct features of a particular episode. The hippocampus is also involved in the recall of previously acquired memories by reactivating the full representations of those memories using partial information as recall cues (pattern completion). This ability of the hippocampus is also important because in real life, specific episodes are rarely replicated in full.

These mnemonic requirements have been suggested to be subserved by specific hippocampal subregions and circuits (Figure 1A). For pattern completion, synaptic transmission and plasticity in the recurrent network of CA3 have been proposed to play a crucial role on a theoretical basis (Marr, 1971; McNaughton and Morris, 1987; O'Reilly and McClelland, 1994; Treves and Rolls, 1994; Hasselmo et al., 1995), and this has been supported by the targeted manipulation of NMDA receptors in CA3 (Nakazawa et al., 2002). Conversely, synaptic transmission and plasticity in the feed-forward pathway from the entorhinal cortex (EC) → dentate gyrus (DG) → CA3 have been implicated in pattern separation based on the spatial and temporal segregation of the initially overlapping EC memory engrams (Marr, 1971; McNaughton and Morris, 1987; O'Reilly and McClelland, 1994; Treves and Rolls, 1994; Leutgeb et al., 2007; Bakker et al., 2008). This hypothesis has been supported by impairments observed in rodents with DG lesions (Gilbert et al., 2001; Hunsaker and Kesner, 2008) as well as mice with a targeted deletion of NMDA receptors in DG granule cells (GCs) (McHugh et al., 2007). These theoretical and experimental studies, however, did not consider the heterogeneity of DG GCs where most GCs (~95%) are generated early during development and do not divide thereafter throughout the animal's life (developmentally born neurons) (Schlessinger et al., 1975; Altman and Bayer, 1990). However, the DG also contains neural progenitor cells that generate GCs throughout life (adult-born neurons), which compose the remaining ~5% of the total GCs in adult animals (Altman and Das, 1965; Eriksson et al., 1998; Gould et al., 1999; Imayoshi et al., 2008). Recently, mice with

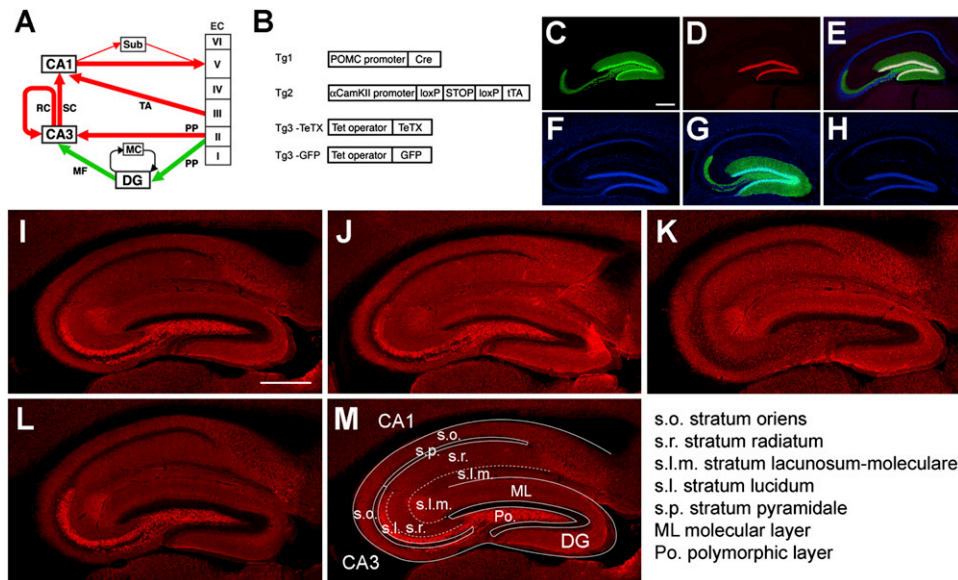


Figure 1. Application of the DICE-K Method to the MF Pathway

(A) Excitatory pathways in the hippocampus and EC. Red and green colors designate alternative pathways.

(B) Transgenic constructs. For the production of the DG-TeTX mouse and the model mouse (DG-GFP), Tg1, Tg2, and Tg3-TeTX mice and Tg1, Tg2, and Tg3-GFP mice were crossed, respectively.

(C–E) A hippocampal section from a DG-GFP mouse raised on Dox, followed by a 2 week Dox withdrawal, costained with anti-GFP (green), anti-Prox1 (a marker for DG GCs [red]), and anti-NeuN (a marker for neurons [blue]). Images shown through a green filter (C), through a red filter (D), and through all three filters (E). (F–H) Hippocampal sections costained with anti-GFP (green) and DAPI (a marker for cell nuclei blue) from a chronically repressed (Dox-on) DG-GFP mouse (F), from a mouse after a 2 week Dox withdrawal (G), and from a mouse in which withdrawal was followed by a 3 week Dox readministration (H).

(I–L) Hippocampal sections stained with anti-VAMP2 from control (I) and DG-TeTX mice (J) both raised on Dox and from a DG-TeTX mouse raised on Dox, followed by a 4 week Dox withdrawal (K) and further followed by a 4 week Dox readministration (L).

(M) Locations of various hippocampal strata.

Scale bars, 500 μ m. See also [Figure S1](#).

reduced adult-born cells were shown to exhibit a deficit in pattern separation (Clelland et al., 2009; Scobie et al., 2009; Tronel et al., 2012), whereas mice with augmented adult neurogenesis were shown to have enhanced pattern separation (Creer et al., 2010; Sahay et al., 2011). These studies left unanswered the function of the vast majority of the GCs generated developmentally. Are they also involved in pattern separation as the theories and earlier experiments suggested? Another unanswered question concerns the age of adult-born GCs. These cells are highly active during the first few weeks after functional integration into the neuronal network (young GCs; Schmidt-Hieber et al., 2004; Ge et al., 2007) but become less active thereafter and functionally indistinguishable from the old developmentally born GCs (together, old GCs; Laplagne et al., 2006). The previous studies did not specify which of the two subsets of adult-born GCs (young or old, or both) is responsible for pattern separation.

To investigate these issues, we created a transgenic mouse in which output of old GCs was specifically inhibited by the tetanus toxin (TeTX) while young GCs (up to 3 to 4 weeks old) were left intact and used context- or space-discriminating memory tasks to examine the pattern separation capability of these mice. These mice exhibited normal or enhanced pattern separation capability between similar contexts that was significantly reduced following removal of young GCs by X-ray irradiation.

Contrary to expectations, mutant mice (no X-ray irradiation) displayed deficits in rapid pattern completion-mediated memory recall.

RESULTS

Generation of Triple-Transgenic Mice

Triple-transgenic DG-TeTX mouse and the triple-transgenic DG-green fluorescent protein (GFP) mouse were generated using the DICE-K method (Nakashiba et al., 2008) (Figure 1B). In the model mouse raised on doxycycline (Dox) followed by a 2 week Dox withdrawal, GFP was expressed robustly and exclusively in the DG throughout the septotemporal axis (Figures S1A and S1B available online). GFP expression was detected in the DG GC layer, the DG molecular layer, and the lucidum of CA3, corresponding to the location of GC dendrites and mossy fibers (MFs), respectively (Figures 1C–1E). GFP expression was repressed under Dox-on conditions (Figure 1F), activated under Dox-on-off conditions (Figure 1G), and re-repressed under Dox-on-off-on conditions (Figure 1H), in which mice were returned to a Dox diet for 3 weeks after 2 weeks of Dox withdrawal.

MF Synaptic Transmission Is Blocked in DG-TeTX Mice

VAMP2's immunoreactivity (IR) can be used as a criterion for transmission at MF-CA3 synapses. VAMP2 IR patterns were

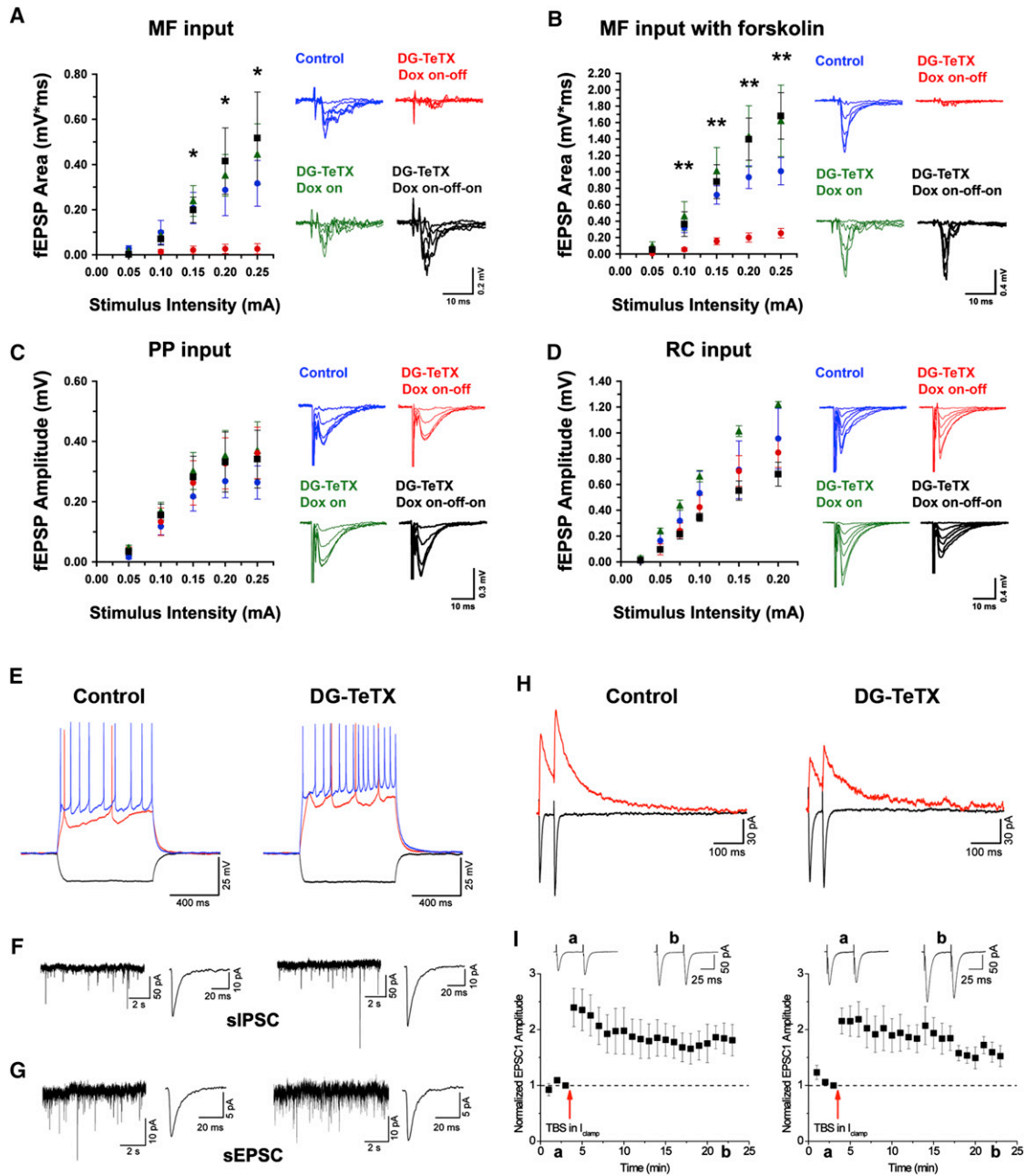


Figure 2. Blockade of MF Synaptic Transmission in DG-TeTX Mice and Comparison of Firing and Synaptic Properties of Young Adult-Born GCs in Control and Activated DG-TeTX Mice

(A and B) I-O relationships of MF input to CA3 in control ACSF (A) and in the presence of forskolin (B).

(C) I-O relationships of the PP input to CA3.

(D) I-O relationships of the RC input to CA3. Blue, control littermates (Tg1×Tg3-TeTX) raised under Dox-on conditions, followed by a 6 week Dox withdrawal; green, repressed DG-TeTX mice (always Dox-on); red, activated DG-TeTX mice raised under Dox-on conditions, followed by a 6 week Dox withdrawal; black, DG-TeTX mice raised under Dox-on conditions, followed by a 6 week Dox withdrawal, followed by a 4 week Dox readministration. For all I-O relations shown, n = 4–7 from at least four different mice per genotype/condition. Representative traces for each condition and pathway are indicated on the right. *p < 0.05, **p < 0.01 between control and activated DG-TeTX mice (t test).

(E–I) Firing and synaptic properties of young (3- to 4-week-old) adult-born GCs in control and activated DG-TeTX mice. (E) Representative traces showing membrane and firing properties of young GCs to hyperpolarizing (–50 pA; black traces) and depolarizing (+50 and +100 pA, red and blue traces, respectively) current injections. (F and G) Representative gap-free traces of pharmacologically isolated spontaneous GABA_A and AMPA receptor-mediated IPSCs (F) and EPSCs (G) with ensemble averages (right traces) in young GCs. (H) Paired-pulse (50 ms interstimulus interval) PP-evoked EPSCs at a holding potential of –70mV (black traces, AMPAR-mediated current) and at a holding potential of +40 mV (red traces, NMDAR-mediated current) in representative recordings from

indistinguishable between the DG-TeTX and control mice (all control mice are of the Tg1×Tg3-TeTX genotype) kept on Dox (Figures 1I and 1J). After 4 weeks of Dox withdrawal, VAMP2 IR was greatly reduced selectively in the stratum (s.) lucidum in DG-TeTX mice (Figure 1K), suggesting an inhibition of synaptic transmission at MF terminals. VAMP2 IR was restored to control levels following a 4 week Dox-on period (Figure 1L).

Synaptic transmission at MF, perforant path (PP), and recurrent (RC) inputs in slices from repressed DG-TeTX and control mice were indistinguishable (Figures 2A, 2C, and 2D). In contrast, slices from activated DG-TeTX mice exhibited severely impaired MF transmission but normal PP and RC transmission (Figures 2A, 2C, and 2D). Importantly, MF excitability was comparable between control, repressed, and activated DG-TeTX mice (Figure S2), confirming that the impaired MF transmission observed in the DG-TeTX mice reflects a deficit in release rather than inefficient fiber stimulation. In contrast to the robust potentiation observed in slices from control and repressed DG-TeTX mice, MF transmission remained barely detectable in slices from activated DG-TeTX mice even when release probability was enhanced with forskolin (Weisskopf et al., 1994) (Figure 2B). As with VAMP2 IR, MF transmission was completely restored in slices from re-repressed DG-TeTX mice (Figures 2A and 2B). Considered together, the *ex vivo* VAMP2 IR and *in vitro* field recording data indicate that MF synaptic transmission in DG-TeTX mice is robustly inhibited by the loss of vesicle fusion selectively at MF terminals in an inducible and reversible manner. Importantly, no detectable abnormalities were found in the cytoarchitecture of MF projections or the hippocampus in activated DG-TeTX mice (Figures S1C and S1D).

MF Synapses of Young Adult-Born GCs Are Intact in DG-TeTX Mice

The generation and survival of adult-born GCs were normal in activated adult DG-TeTX mice (Figures S3A–S3C). Moreover, the differentiation of neural progenitor cells in activated DG-TeTX mice produced normal proportions of GCs and glia (Figures S3D–S3G). A genetically engineered Moloney viral vector (Figure 3A) was injected into the DGs of activated DG-TeTX mice and control littermates to selectively label MF boutons from adult-born GCs (van Praag et al., 2002) and examine whether the transmissions at these synapses are inhibited (Figure 3B). Three weeks after the viral injection (Figures 3C and 3D), numerous mCherry-fused VAMP2-positive puncta (mCheV2, red) appeared in CA3 s. lucidum (where MFs should synapse onto CA3 cells). These puncta were superimposed nearly perfectly with GFP-fused synaptophysin (SypGFP, green) in both activated DG-TeTX mice and control littermates, with no discernable difference between the two genotypes. Conversely, 6 weeks after the injection (Figure 3E), the proportion of SypGFP-positive puncta colocalized with mCheV2 was substantially reduced in only the activated DG-TeTX mice. A

gradual decrease of this proportion over the ages of the adult-born GCs was observed (Figure 3F), suggesting that synaptic transmission at MF terminals of young adult-born GCs (up to 3 weeks old) was relatively intact, although it gradually decreased as the cells became older (Figure 3F). This conclusion was supported by the lack of GFP expression in the adult-born doublecortin (DCX)-positive GCs (a marker for up to 3-week-old cells) (Nacher et al., 2001; Snyder et al., 2009) in the DG-GFP mice (Figures 3G–3K). Additional experiments using wheat germ agglutinin (WGA), a synaptic vesicle fusion-dependent anterograde *trans*-synaptic marker (Tabuchi et al., 2000; Braz et al., 2002), demonstrated that synaptic transmission from 4-week-old adult-born GCs was intact, at least in the hilar region, in activated DG-TeTX mice (Figures S3H–S3L).

Young Adult-Born GCs in DG-TeTX Mice Receive Functional Synaptic Inputs, and Their Functions Are Unaffected by the TeTX Manipulation

To examine synaptic inputs to young (3-week-old) adult-born GCs, we injected another Moloney virus (Figure 4A, Virus 1A) and an engineered rabies virus (Figure 4B, Virus 2) (Wickersham et al., 2007) into the DGs of activated DG-TeTX mice and control littermates (see Experimental Procedures). In a control hippocampal section, nearly all GFP-positive (i.e., TVA- and rabies G-positive) young adult-born GCs had red fluorescent protein (RFP) signal derived from Virus 2 as a result of direct interaction between EnvA and TVA (Figure 4C). With the complementation of rabies G in the GFP-positive GCs, monosynaptic retrograde labeling occurred extensively in the hilar region and sparsely in CA3, where the RFP signal never overlapped with GFP, excluding the possibility of direct Virus 2 infection into those cells (Figure 4C). RFP signal was also detected in NeuN-positive neurons of EC superficial layer II with dendrites extending toward layer I (Figures 4E and 4G). RFP signal was rarely detected in cells other than GFP-positive GCs when rabies G was not provided by a Moloney virus (Figure 4A, Virus 1B), further confirming the specificity of retrograde labeling (Figures 4D and 4F). In activated DG-TeTX mice, there was no discernable difference from control mice in brain areas where cells were retrogradely labeled from young 3-week-old adult-born GCs (Figures 4C, 4E, and 4G), indicating that young adult-born GCs in DG-TeTX mice receive synaptic inputs.

We compared the intrinsic membrane and synaptic properties of young adult-born GCs in control and activated DG-TeTX mice. Mice (3 to 4 months old) were infected with Moloney virus encoding GFP and sacrificed 3–4 weeks later for whole-cell patch clamp recordings from GFP-labeled GCs in acute hippocampal slices (Figures 2E–2I). No genotype-specific differences were observed between GFP-labeled GCs for any of the basic membrane and spiking properties, including resting membrane potential, input resistance, membrane time

young GCs. (I) Pooled data showing long-term potentiation of PP-evoked AMPAR-mediated EPSCs in response to a theta burst induction protocol (see Experimental Procedures) in young GCs in control (n = 8) and activated DG-TeTX mice (n = 6). Inset traces a and b show EPSCs taken at the time indicated on the x axes.

Data represent mean ± SEM. See also Figure S2 and Table S1.

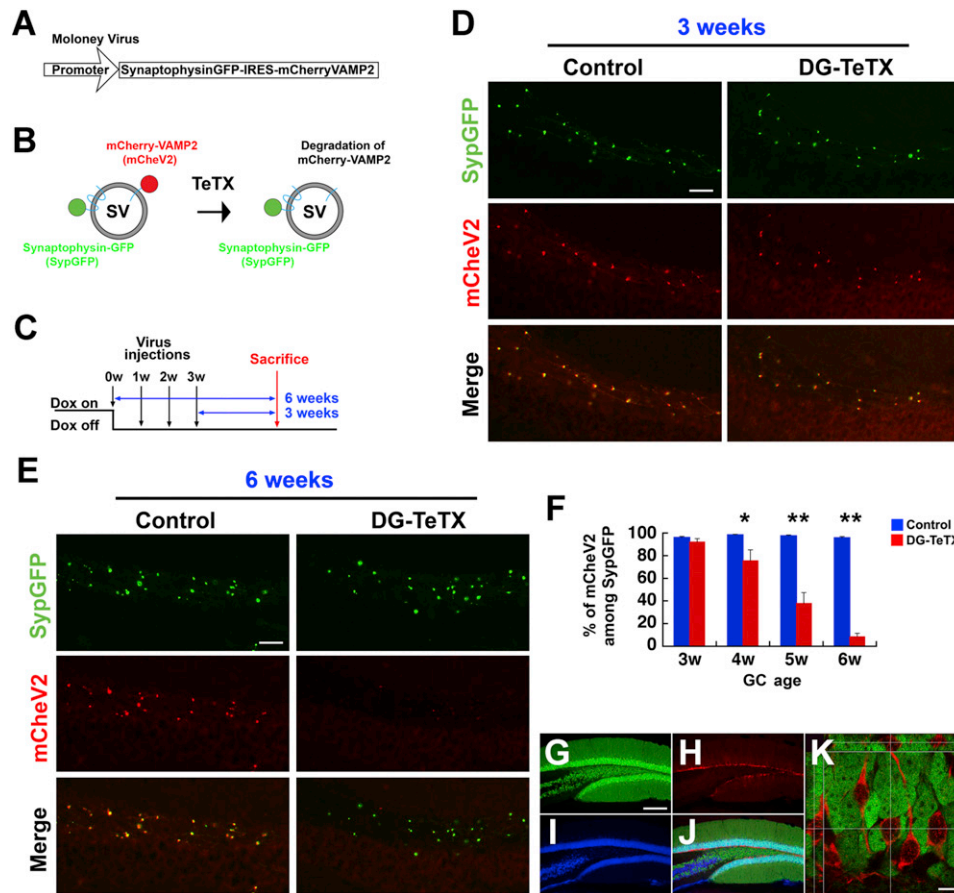


Figure 3. Integrity of MF Transmission from Young Adult-Born GCs

(A) A Moloney viral vector encoding bicistronic SypGFP and mCheV2.

(B) SypGFP- and mCheV2-labeled synaptic vesicles (SV). TeTX cleaves the mCheV2, leading to loss of mCheV2 immunoreactivity.

(C) Dox diet, viral injection, and mouse sacrifice schedules.

(D and E) Presence of VAMP2 at MF boutons from 3-week-old adult-born GCs (D) and its absence at MF boutons from 6-week-old adult-born GCs (E). S. lucidum areas of hippocampal sections stained with anti-GFP (green) and anti-mCherry (red) from control and activated DG-TeTX mice are shown.

(F) Proportion of mCheV2-positive puncta among SypGFP-positive puncta at various GC ages. At least three different mice per genotype/condition were used. * $p < 0.05$ for 4-week-old GCs; ** $p < 0.01$ for 5- and 6-week-old GCs (t test).

(G–K) A hippocampal section from a DG-GFP mouse costained with anti-GFP (green, G), anti-DCX (red, H), and anti-NeuN (blue, I; merge, J). (K) A confocal image at a single z axis with green and red filters. Optical sections along the horizontal or vertical lines across multiple z axes are shown on the top and left, respectively. Scale bars in (D) and (E), 25 μm ; (G)–(J), 250 μm ; (K), 10 μm . Data represent mean \pm SEM. See also Figure S3.

constant, and spike frequency/duration (Figure 2E and Table S1). GFP-labeled cells received both GABAergic inhibitory and glutamatergic excitatory synaptic input (Figures 2F and 2G and Table S1), indicating that the synapses observed with rabies virus (Figure 4) were functional. Importantly, comparison of control and DG-TeTX young adult-born GCs revealed no differences in any of the synaptic properties assayed, including inhibitory/excitatory postsynaptic current kinetics, AMPA/NMDA ratios, and short- or long-term synaptic plasticity at PP inputs (Figures 2H and 2I and Table S1). Together, these findings confirm that adult-born GCs are synaptically integrated into the entorhinal-hippocampal circuitry by 3–4 weeks of age, and that blockade of transmission in the developmentally born GCs does not alter the electrophysiological and synaptic properties of young adult-born GCs.

Contextual Discrimination Is Enhanced in DG-TeTX Mice for a Highly Similar Context Pair

Activated DG-TeTX mice did not exhibit detectable abnormalities in anxiety, locomotor activity, motor coordination, or pain sensitivity (Figure S5). In contextual fear conditioning, the activated DG-TeTX mice froze similarly to control mice (Figure 5A, analysis of variance [ANOVA], genotype: $F_{(1,22)} = 0.145$, $p = 0.707$), and they exhibited no deficit in distinguishing a pair of relatively distinct contexts, A and D, (Figure 5B, ANOVA, context: $F_{(1,22)} = 107.13$, $p < 0.0001$; genotype: $F_{(1,22)} = 0.155$, $p = 0.698$; context \times genotype: $F_{(1,22)} = 2.145$, $p = 0.157$). We then subjected another cohort to a contextual discrimination fear conditioning (McHugh et al., 2007) in which mice learned to discriminate a pair of very similar contexts over repeated trials with a single footshock in one of the contexts (shock context; A).

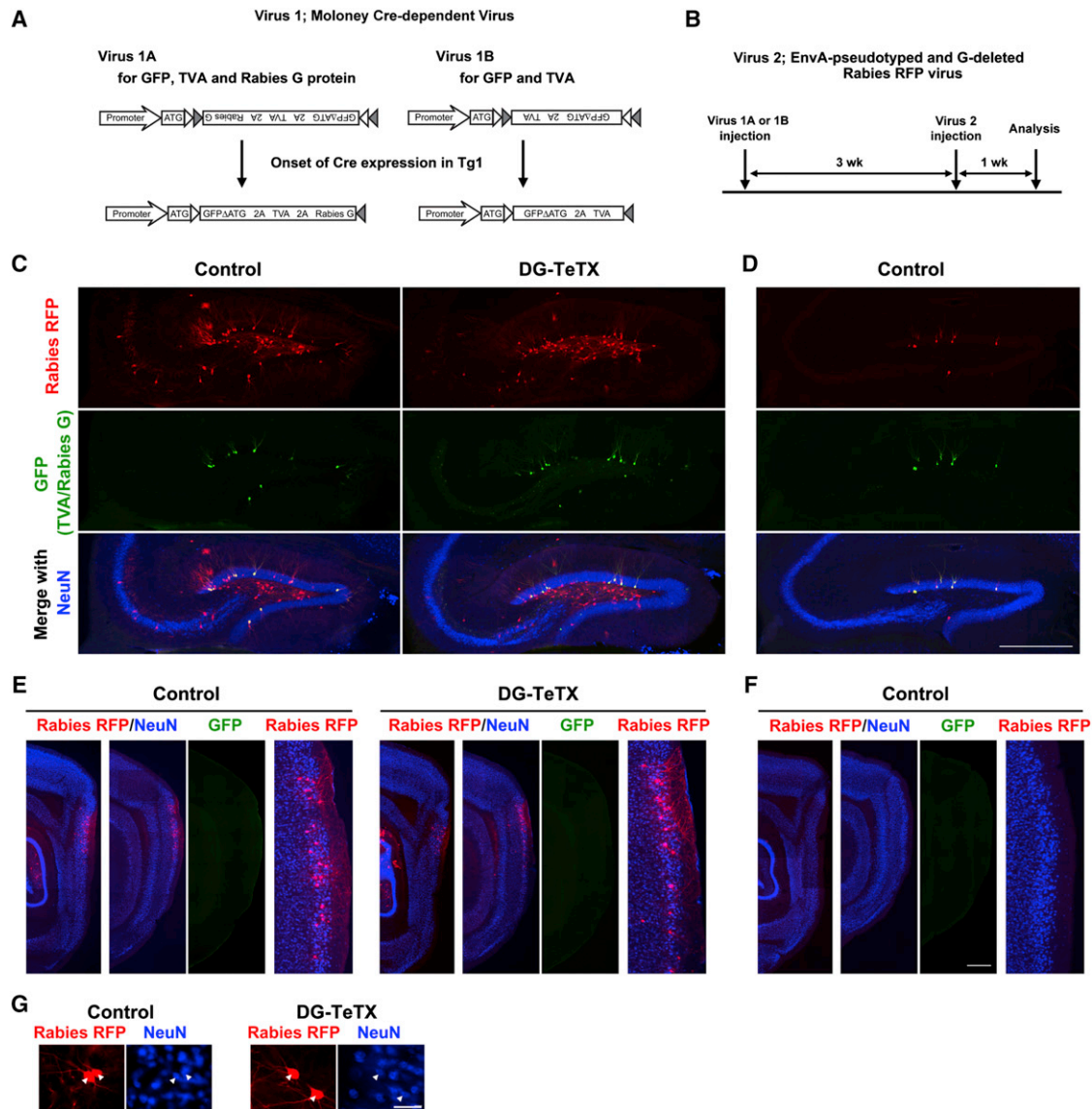


Figure 4. Young Adult-Born GCs Receive Synaptic Inputs

(A) Two different Cre-dependent Moloney viral vectors. Virus 1A (left) expresses GFP, TVA (a receptor for EnvA), and rabies G glycoprotein, whereas Virus 1B (right) expresses GFP and TVA. Cre-loxP recombination by Tg1 occurs between 1 and 2 weeks after the Moloney virus injection (Figure S4).

(B) Schedule of analysis relative to viral injections.

(C) Hippocampal sections from control and activated DG-TeTX mice injected with Virus 1A and Virus 2 costained with anti-RFP (red), anti-GFP (green), and anti-NeuN (blue).

(D) A hippocampal section from a control mouse injected with Virus 1B and Virus 2.

(E) Parasagittal sections at two different mediolateral levels covering the EC (first and second columns) from control and activated DG-TeTX mice injected with Virus 1A and Virus 2. GFP images (third column) are taken from sections shown in the second column. High-magnification images of the EC superficial layers (fourth column) are from images in the second column.

(F) Parasagittal sections from a control mouse injected with Virus 1B and Virus 2.

(G) RFP- and NeuN-positive cells (arrowheads) in the EC.

Scale bars in (C)–(F), 500 μ m; (G), 50 μ m. See also Figure S4.

The other context (safe context; B) shared nearly all features with A, except that the sidewalls in B sloped inward at a 60° angle from the floor. This task, in which DG-NR1 mice are known to be impaired (McHugh et al., 2007), requires mice to respond to two similar patterns based on their memory of previous experi-

ences with those patterns. On the first 3 days, the mice were placed only into A, receiving a footshock after 180 s. Freezing levels were assessed for the first 3 min before shock delivery (Figure 5C). During conditioning, activated DG-TeTX mice acquired fear memory to A similar to control mice (Figure 5C,

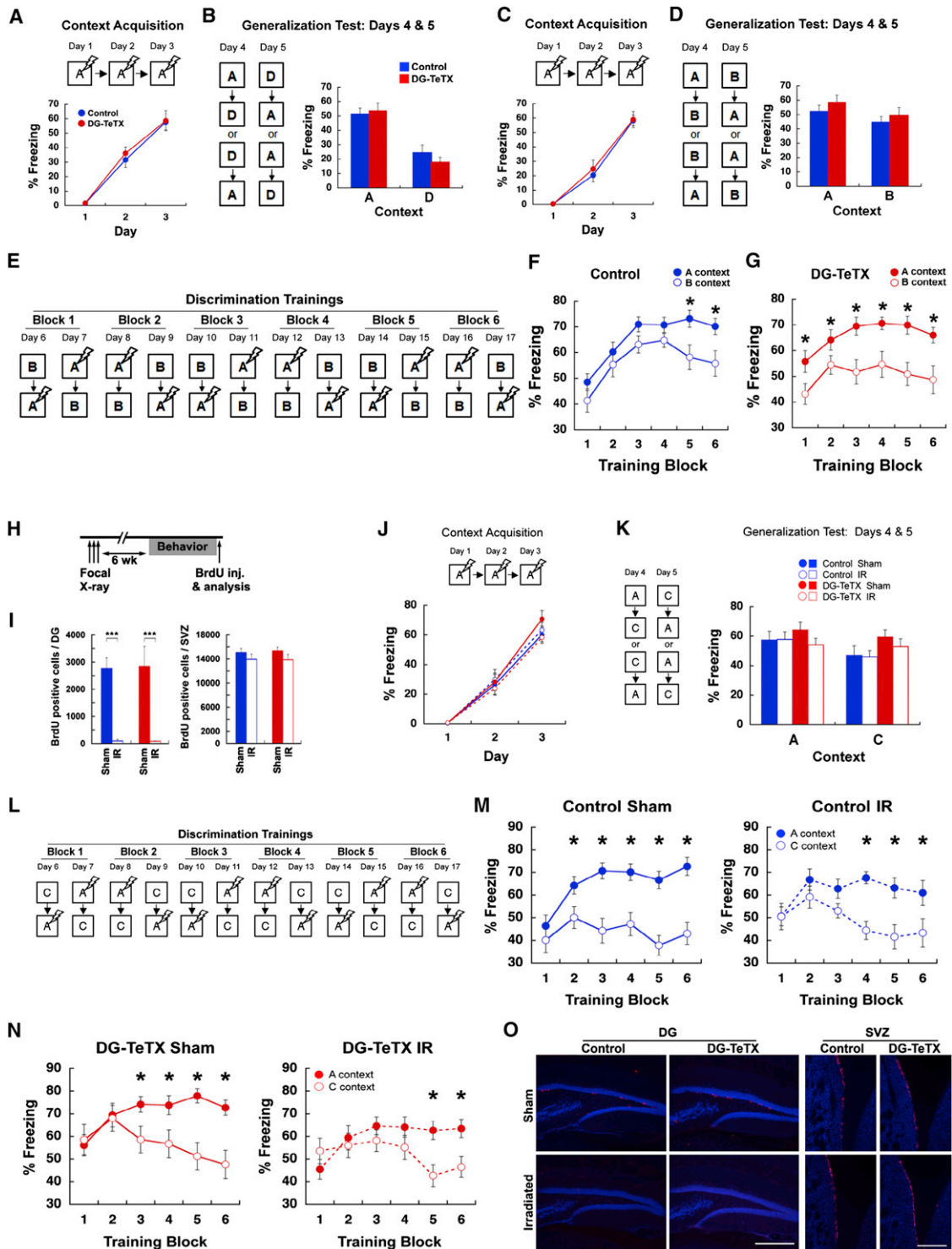


Figure 5. DG-TeTX Mice Show Enhanced Contextual Discrimination in a Highly Similar Context Pair, and Their Intact Young GCs Are Necessary for This Discrimination

(A and B) Contextual discrimination between a very distinct context pair, A and D. (A) Freezing levels during the acquisition (blue, control; red, DG-TeTX; n = 12 per genotype). (B) Freezing levels in A and D during the generalization test.

(C–G) Another set of mice (n = 12 per genotype) were subjected to contextual discrimination between a very similar context pair, A and B. (C) Freezing levels during the acquisition. (D) Freezing levels in A and B during the generalization test. (E) Experimental procedure for discrimination training between A and B. (F and G) Freezing levels in A (filled circles) and B (open circles) of control (blue, F) and DG-TeTX mice (red, G).

ANOVA, genotype: $F_{(1,22)} = 0.140$, $p = 0.712$). Context specificity was tested on days 4 and 5, when the mice of each genotype were divided into two groups. One group visited A then B on day 4 and visited B then A on day 5. The other group visited the contexts in the opposite order. Neither group received a shock in A or B (Figure 5D). Mice froze somewhat more in the shock context (A) than in the nonshocked context (B). Both genotypes showed robust and equivalent generalization between contexts, and no discernable differences in freezing were observed (Figure 5D, ANOVA, context: $F_{(1,22)} = 4.867$, $p < 0.04$; genotype: $F_{(1,22)} = 2.162$, $p = 0.156$; context \times genotype: $F_{(1,22)} = 1.023$, $p = 0.323$). The mice were subsequently trained to discriminate these contexts by visiting the two contexts daily for 12 days, always receiving a footshock 180 s after being placed in A but not B (Figure 5E). As shown in Figures 5F and 5G, only activated DG-TeTX mice exhibited significant discrimination across all trial blocks, whereas controls did not acquire significant discrimination until the final two trial blocks. Thus, the loss of MF transmission in developmentally born GCs and older adult-born GCs resulted in *no* deficit in the discrimination of highly similar contexts but rather an enhanced discrimination compared to control mice.

Contextual Discrimination Depends on Young Adult-Born GCs in Both DG-TeTX and Control Mice

We next ablated adult-born DG GCs by irradiating activated DG-TeTX mice and control littermates with X-ray (Santarelli et al., 2003) (Figures 5H, 5I, and 5O) and subjected the irradiated (IR) and sham-operated (Sham) mice to contextual discrimination fear conditioning (Figures 5J–5N). Given that the previously used highly similar context pair (A versus B) was difficult for control mice to discriminate (Figure 5F), we chose to use a more distinct yet similar context pair to test the role of adult-born GCs in pattern separation, thus allowing for a clearer detection of potential discrimination deficits. The context pair used (A versus C) was located in the same room and differed in odor and background noise, in addition to differing sidewalls (which were the only feature that differed between the highly similar pair, A and B). All four groups acquired a similar fear memory to A (Figure 5J, ANOVA, genotype: $F_{(1,52)} = 0.314$, $p = 0.578$; irradiation: $F_{(1,52)} = 0.350$, $p = 0.350$; genotype \times irradiation: $F_{(1,52)} = 2.487$, $p = 0.121$) and showed strong generalization to C over the 2 day generalization test (ANOVA, context: $F_{(1,52)} = 22.578$, $p < 0.001$). However, DG-TeTX mice showed a slight, but significant, elevation in generalization to context C (ANOVA, context \times genotype: $F_{(1,52)} = 7.296$, $p < 0.009$), and this was not affected by irradiation (Figure 5K, ANOVA, context \times genotype \times irradiation interaction: $F_{(1,52)} = 0.725$, $p = 0.398$). During discrimination trainings (Figures 5L–5N), Sham control mice began to discrimi-

nate A and C on trial block 2, three blocks earlier than the A versus B discrimination (Figure 5F). In contrast, IR control mice did not discriminate until trial block 3 (Figure 5M), confirming that adult-born GCs are important for efficient discrimination. The irradiation effect was also observed in activated DG-TeTX mice (Figure 5N). Sham DG-TeTX mice began to discriminate on trial block 3 (one block later than Sham control mice), whereas IR DG-TeTX mice were unable to discriminate until trial block 5, therefore exhibiting the worst discrimination efficiency among the four groups and indicating that young adult-born GCs in activated DG-TeTX mice are crucial for the contextual discrimination observed in these mice.

Spatial Discrimination Is Normal in DG-TeTX Mice

For another test of behavioral discrimination, we used a delayed nonmatching to place (DNMP) task in an eight-arm radial maze. Mice with reduced hippocampal adult neurogenesis were previously shown to be impaired in this task when the reward arm was relatively close to the sample arm (Clelland et al., 2009). Conversely, our present data show that activated DG-TeTX mice made correct choices as efficiently as control mice regardless of the angles separating the sample and reward arms (Figures 6A–6C, $p > 0.05$ for comparison between genotypes in each separation, t test), indicating that MF inputs from the vast majority of GCs are dispensable for spatial pattern separation.

Rate Remapping in the Hippocampus Is Normal in DG-TeTX Mice

To obtain a physiological correlate of the normal spatial discrimination observed in the DG-TeTX mice, we investigated possible changes in the ensemble activity in CA3 and CA1 while animals foraged in a novel arena after exploring a similar but distinct familiar environment set in the same room (Figures 6D–6G and Table S2). Neuronal ensembles in the CA3 region of DG-TeTX mice exhibited intact rate remapping between the contexts compared to control animals (Figure 6F, ANOVA, genotype \times region: $F_{(1,428)} = 0.27$, $p = 0.62$; genotype: $F_{(1,428)} = 1.66$, $p = 0.19$; region: $F_{(1,428)} = 13.09$, $p < 0.001$; Bonferroni post-test, control CA1 \times control CA3, $p < 0.05$; DG-TeTX CA1 \times DG-TeTX CA3, $p < 0.001$). The rate differences in CA3 of both DG-TeTX and control mice were what would have been expected from the formation of an independent representation ($p > 0.05$ for control and DG-TeTX, t test), but CA1 rate differences were not ($p = 0.012$ and $p < 0.001$ for control and DG-TeTX, respectively, t test). Figure 6G shows the cumulative probability histogram for the rate overlap in the CA3 and CA1 regions. Importantly, no genotype-specific differences were observed in either CA3 or CA1 ensembles

(H–O) Activated DG-TeTX and control littermates with either IR or Sham ($n = 14$ per group) were subjected to contextual discrimination between a slightly distinct context pair, A and C. (H) Mice were focally irradiated 6 weeks prior to contextual discrimination fear conditioning. (I) The number of BrdU-positive cells in the DG and in the subventricular zone (SVZ; blue, control; red, DG-TeTX; *** $p < 0.001$ in both genotypes, t test). (J) Freezing levels during the acquisition (blue, control; red, DG-TeTX; filled circles and solid lines, Sham; open circles and broken lines, IR). (K) Freezing levels in A and C during the generalization test. (L) Experimental procedure for discrimination trainings between A and C. (M and N) Freezing levels in A (filled circles) and C (open circles) of control (M) and DG-TeTX mice (N). (O) DG and SVZ areas of sections stained with anti-BrdU (red) and anti-NeuN (blue). * indicates Scheffé's correction for multiple comparison, $p < 0.05$. Scale bars in (O), 500 μm .

Data represent mean \pm SEM. See also Figure S5.

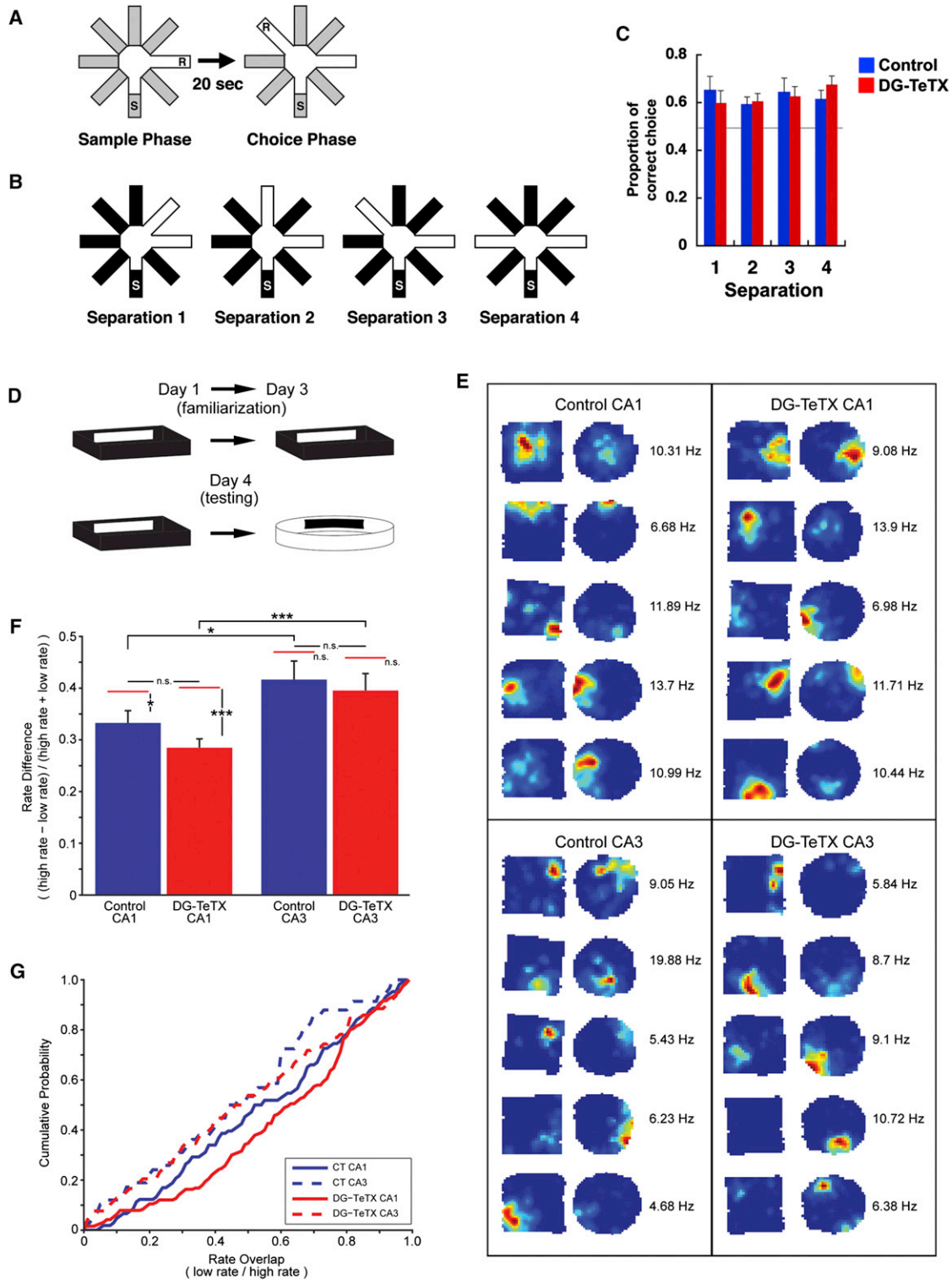


Figure 6. Normal Spatial Discrimination and Normal Rate Remapping in DG-TeTX Mice

(A) Pattern separation was tested using a DNMP protocol by varying angles between sample and reward arms (S, start arm; R, reward; see [Experimental Procedures](#)).

(B) Two arms were separated by 45°, 90°, 135°, and 180° in separations 1–4, respectively.

(C) Proportions of correct choices as a function of arm separation angles. The horizontal gray line represents chance. n = 12 per genotype.

(D) Example of behavioral pattern separation paradigm.

(Mann-Whitney U-test; $p > 0.05$), yet in both genotypes, similar differences were observed between the regions (Mann-Whitney U-test; $p < 0.05$ and $p < 0.01$, respectively). These physiological data support the behavioral data from the spatial discrimination task and the conclusion that output from the vast majority of DG GCs (i.e., old GCs) is not necessary for spatial pattern separation.

Rapid Pattern Completion-Mediated Contextual Recall Is Impaired in DG-TeTX Mice

The pre-exposure-dependent contextual fear conditioning paradigm (Fanselow, 1986, 1990) has been used previously to test a rodent's ability to carry out pattern completion-based memory recall (Matus-Amat et al., 2004; Nakashiba et al., 2008). Figure 7A summarizes the protocols for the experimental and control groups (see Experimental Procedures). At the probe test, activated DG-TeTX mice displayed a freezing deficit (Figure 7B, $p < 0.01$, t test) that was likely due to the animals' inability to rapidly (10 s re-exposure to a context) recall a full contextual representation previously formed (presumably in CA3) during pre-exposure under normal MF transmission, as the freezing deficit was not present when the context re-exposure time was prolonged to 3 min (Figures 7B and 7C, ANOVA, genotype \times time: $F_{(1,115)} = 4.647$, $p = 0.033$; Bonferroni post-test, $p > 0.05$ between genotypes in Figure 7C). The freezing deficit was also not seen in DG-TeTX mice when conditioning occurred under the Dox-on condition (Figures 7B and 7D, ANOVA, genotype \times Dox condition: $F_{(1,115)} = 4.107$, $p = 0.045$; Bonferroni post-test, $p > 0.05$ between genotypes in Figure 7D). When the pre-exposures were to a distinct context (Figure 7E), freezing levels were similar to controls not given a foot-shock (Figure 7F, ANOVA, genotype \times condition: $F_{(1,44)} = 0.050$, $p = 0.8233$; genotype: $F_{(1,44)} = 0.019$, $p = 0.900$; condition: $F_{(1,44)} = 0.161$, $p = 0.690$). It is possible that the contextual memory engram acquired under Dox-on conditions may have been degraded during the subsequent 4-week-long Dox-off period. However, when we measured contextual fear memory in DG-TeTX mice 4 weeks after conditioning, we found no genotype-specific difference in freezing levels (Figures S6A and S6B). These results indicate that MF output from the developmentally born GCs and/or older adult-born GCs is crucially involved in rapid pattern completion-mediated recall of contextual memories.

Rapid Pattern Completion-Mediated Spatial Recall Is Impaired in DG-TeTX Mice

We next subjected mice to the standard water maze task in which the spatial memory was tested with varying degrees of distal cue availability (Figures 7G and 7H). DG-TeTX mice learned the location of the hidden platform with kinetics indistin-

guishable from control littermates under the Dox-on and full-cue conditions (Figure 7I, ANOVA, genotype: $F_{(1,45)} = 0.027$, $p = 0.870$). We did not observe any genotype-specific differences in distance traveled or swim speed (Figures S7A and S7B). During the probe trials, we used the latency to reach the phantom platform the first time as the measure of rapid memory recall (Nakazawa et al., 2002; Slutsky et al., 2010). In the probe trial conducted at the end of the training session (P1, Dox-on), we did not detect any genotype-specific differences in the latencies (Figure S7C). Following 5 weeks of Dox withdrawal, we subjected the mice to successive probe trials under partial-cue conditions, one trial per day. The latencies were significantly longer in activated DG-TeTX mice compared to controls in the one-cue probe trial (P2, Figures 7J and 7K, $p < 0.05$, t test), and there were longer, though not significant, latencies for mutants in the two-cue probe trial (P3, Figures 7J and 7K, $p > 0.05$, t test). These prolonged latencies were not due to enhanced memory extinction in the mutants because in the full-cue probe trial conducted 1 day later, the mutants' latencies were comparable to those of controls (P4, Figures 7J and 7K), which were not significantly different from the latencies observed in P1 (ANOVA, genotype \times probe trials: $F_{(1,45)} = 0.004$, $p = 0.652$; genotype: $F_{(1,45)} = 1.203$, $p = 0.279$; probe trials: $F_{(1,45)} = 1.986$, $p = 0.166$). Furthermore, the longer latencies observed in the mutants under the P2 condition were not due to a deficiency in swimming, as the swim speeds in the mutants were similar to those of controls in the full-cue probe trial (P4, Figure S7E). The latencies observed in P2, P3, and P4 indicate that while the control mice can recall the memory under partial-cue conditions as well as the full-cue condition, the mutants' recall ability is sensitive to the extent of cue availability (ANOVA, probe trials: $F_{(2,45)} = 5.777$, $p = 0.004$; Bonferroni post-test, $p > 0.05$ for comparison of pairs among P2, P3, and P4 in both genotypes, except $p < 0.01$ for P2 versus P4 in DG-TeTX mice). In the probe trial conducted with none of the four distal cues 1 day after the full-cue probe trial (i.e., P5), both genotypes showed similar latencies (Figure S7D). In control mice, the latency in P5 was significantly longer than any of the latencies observed under the other conditions (ANOVA, probe trials: $F_{(3,45)} = 17.92$, $p < 0.0001$; Bonferroni post-test, $p < 0.001$ for comparison of P2, P3, or P4 to P5). In contrast, mutants' latencies in P5 were indistinguishable from those in P2 (Bonferroni post-test, $p > 0.05$ for P2 versus P5) but significantly longer than those in P3 or P4 (Bonferroni post-test, $p < 0.01$ for P3 versus P5; $p < 0.001$ for P4 versus P5). We also measured the spatial memory under the partial-cue condition using the 90 s platform occupancy test and found no genotype-specific or cue paucity-dependent deficits (Figures S7F and S7G). Thus, when sufficient time is allowed, the mutant mice can recall the location of the phantom platform under the partial-cue condition. These results indicate that the

(E) Place field examples from control (left) and DG-TeTX mice (right) for CA1 (top) and CA3 (bottom) pyramidal cells. The two maps from each example were normalized to the maximum peak firing rate between the maps, indicated to the right of each pair.

(F) Rate remapping index for place cells recorded from CA1 (left) and CA3 (right) regions of control (blue) and DG-TeTX mice (red). There was a similar significant difference in rate between CA1 and CA3 in control and DG-TeTX mice ($*p < 0.05$ and $***p < 0.001$, respectively, t test). The red bars above each column represent the estimated rate difference (ERD) expected given independent firing in the two boxes for that region/genotype. Only significant differences were observed between the actual and ERD in the CA1 regions of control and DG-TeTX mice ($*p = 0.012$ and $***p < 0.001$, respectively, t test).

(G) Cumulative probability histograms of the overlap values (low rate/high rate) for each genotype and region.

Data represent mean \pm SEM. See also Table S2.

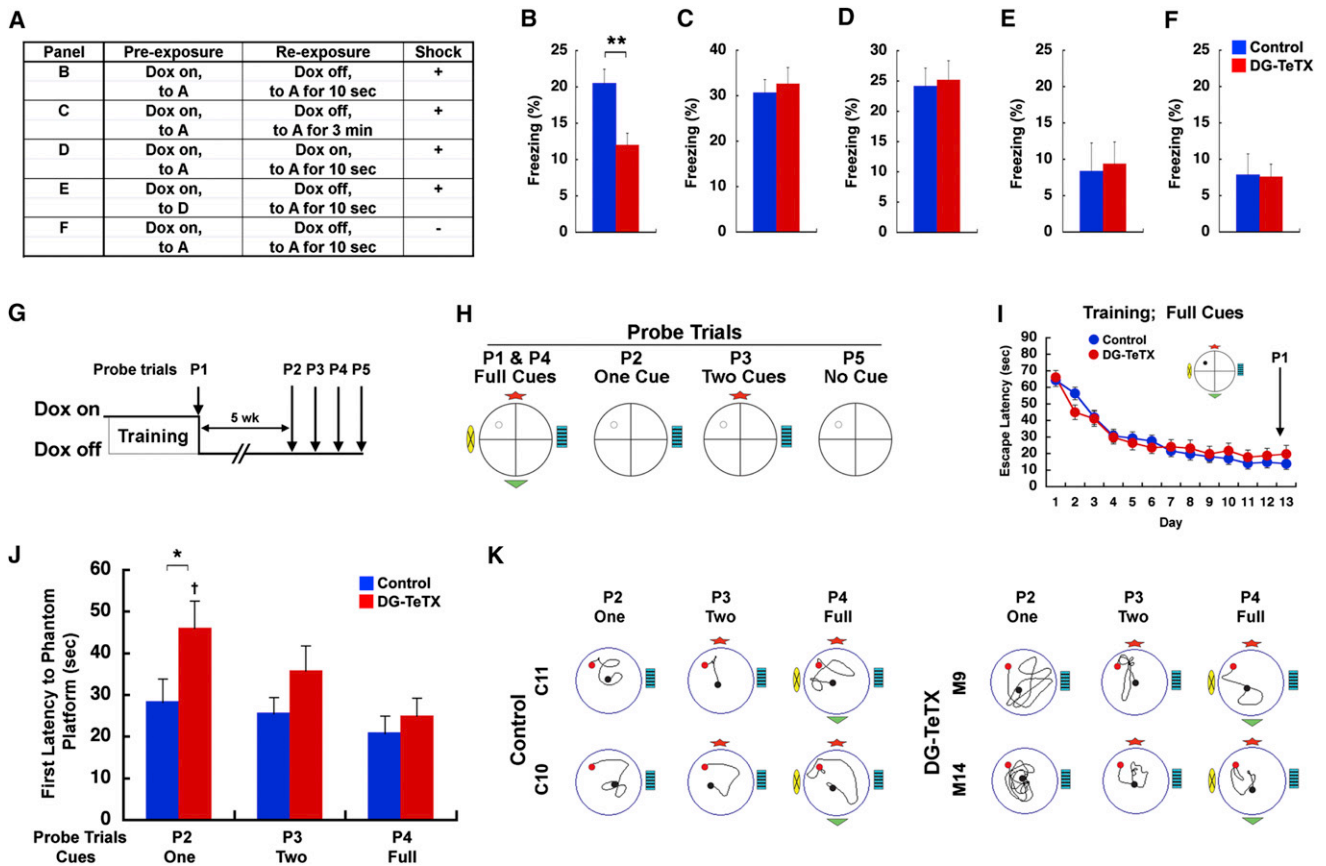


Figure 7. DG-TeTX Mice Exhibit Deficits in Pattern Completion-Mediated Contextual and Spatial Recall

(A–F) Pre-exposure-dependent contextual fear conditioning. (A) Experimental procedure for (B)–(F). Repressed DG-TeTX and control littermates were subjected to a pre-exposure session (for 5 consecutive days, 10 min per day) in either context A or D. The mice were then shifted to a Dox-free diet (except in D). Next, the mice were (re)-exposed to context A and then received a single footshock within either 10 s or 3 min. Mice in (F) did not receive a footshock. (B–F) Freezing levels in context A measured 1 day after (re)-exposure (blue, control; red, DG-TeTX). $n = 35$ and 36 in (B) for DG-TeTX mice and control mice, respectively; $n = 24, 24, 12$, and 12 for both genotypes in (C), (D), (E), and (F), respectively; $**p < 0.01$, t test.

(G–K) Spatial memory recall with various cue conditions in the standard Morris water maze task. (G) Experimental procedure. Repressed DG-TeTX ($n = 23$) and control littermates ($n = 24$) were trained to locate a hidden platform location in the full-cue condition. The mice were then switched to a Dox-free diet. The P1 probe trial was conducted under the Dox-on condition, whereas the P2–P5 probe trials were conducted under the Dox-off condition. (H) Probe trials with cue manipulation. (I) Escape latencies to the hidden platform during the training (blue, control; red, DG-TeTX). (J) First latencies to the phantom platform during the probe trials. (K) Examples of the swim path to the phantom platform (red) for the probe trials (the black circle represents the start point). $*p < 0.05$; $\dagger p < 0.01$ in DG-TeTX mice, P2 versus P4.

Data represent mean \pm SEM. See also Figures S6 and S7.

mutants’ deficits are in the speed of pattern completion recall rather than in its capacity. Our results suggest that the MF input from old GCs promotes this specific aspect of pattern completion-mediated recall.

DISCUSSION

Because the properties of mutants’ dentate GCs are crucial for the interpretation of behavioral and in vivo physiological data, we first used in vitro electrophysiology and cell biology to characterize them. Our data indicated that in the mutants, transmission is robustly and specifically inhibited at most MF-CA3 synapses under the Dox-off condition (Figure 2). Our data also demonstrated that 3- to 4-week-old adult-born GCs are functionally integrated into the network, and that the physiological

properties of these adult-born GCs are not affected by lack of MF transmission of the majority of GCs (Figures 2, 3, 4, and S3). The MF-CA3 contacts of the young adult-born GCs, however, gradually declined after 4 weeks of age with about 5% remaining intact at 6 weeks of age (Figures 3E and 3F). It is known that adult-born dentate GCs are highly excitable and exhibit greater synaptic plasticity compared to the numerically dominant developmentally born (and hence older) GCs (Schmidt-Hieber et al., 2004; Ge et al., 2007) up to ~6 weeks of cellular age and thereafter become less active and indistinguishable from developmentally born GCs (Laplagne et al., 2006). Therefore, it seems that the TeTX manipulation in the DG-TeTX mice spared a substantial portion of the highly excitable and synaptically plastic young adult-born GCs while inhibiting the MF transmission of most of the developmentally born

GCs and less active older (>6 weeks of age) adult-born GCs. In the remaining discussion, we refer the 3- to 4-week-old adult-born GCs as young GCs and the combined developmentally born and older adult-born GCs as old GCs.

Overall, our results indicate that old GCs do not play a critical role in pattern separation between similar environments but are required for attaining a normal level of rapid pattern completion. These findings were unexpected given that previous theoretical and experimental work has suggested that the EC→DG→CA3 pathway is crucial for pattern separation (Marr, 1971; McNaughton and Morris, 1987; Treves and Rolls, 1994; Gilbert et al., 2001; Leutgeb et al., 2007; McHugh et al., 2007; Hunsaker and Kesner, 2008) and has focused less on its contributions to pattern completion, although it has been suggested that pattern completion could be associated with the strengthening of EC→DG synapses (O'Reilly and McClelland, 1994).

Our current study combined with the recent studies focusing on the role of adult-born DG GCs (Clelland et al., 2009; Scobie et al., 2009; Tronel et al., 2012) provide several new concepts and clarifications regarding the function of the EC→DG→CA3 pathway in episodic memory. First, the lack of MF input from old DG GCs did not impair discrimination of similar contexts or spaces (Figures 5C–5G and 6A–6C), indicating that, under these conditions, neither the greater number nor sparse activity of DG GCs compared to cells in the superficial layers of the EC (Amaral et al., 1990; Jung and McNaughton, 1993), on which most models are based, is sufficient for pattern separation of similar contexts or spaces. This point is important because it is often under these circumstances that we rely on our pattern separation capability for guiding intelligent behavior. Second, we observed a trend indicating that old GCs may be involved in the discrimination of relatively distinct contexts (compare Figures 5G and 5N), suggesting that the spatial and temporal dispersion of memory-encoding cells as the information flows from the EC to DG followed by its orthogonalization from DG to CA3 (McNaughton and Morris, 1987; Treves and Rolls, 1994) may contribute to pattern separation of relatively distinct contexts. Third, we confirmed by X-ray irradiation that adult-born DG GCs are crucial for efficient acquisition of the contextual discrimination power in normal mice (Scobie et al., 2009; Tronel et al., 2012; Sahay et al., 2011). Additionally, we demonstrated that it is the young adult-born GCs that are required for the discrimination of similar contexts. Fourth, among the four groups used in the X-ray irradiation experiments, the IR DG-TeTX mice exhibited the lowest efficiency in contextual discrimination (Figures 5M and 5N). These mice lack functional MF transmission from both developmentally born and adult-born GCs, leaving only the direct PP input to CA3 from EC layer II. Thus, our results suggest that this input does not support pattern separation. Finally, regarding the discrepancies between the present work and previous lesion-based studies (Kesner, 2007; Lee and Kesner, 2004), lesions would have damaged the output of both young and old GCs and therefore would not have permitted the elucidation of their differential roles. Likewise, the contextual discrimination and the rate-remapping deficits observed in DG-NR1 knockout (KO) mice (McHugh et al., 2007) could be due to the inhibition of synaptic plasticity in young GCs because the

POMC promoter is active in these cells (Figure S4) (Overstreet et al., 2004).

The enhanced contextual discrimination in activated DG-TeTX mice was observed only when a highly similar pair of contexts was used for contextual fear conditioning (Figures 5F and 5G). At the moment, we can only speculate how this phenomenon occurred under these conditions. One possibility is that pattern completion and separation are counteractive in control mice and that the deficit in the former led to an enhancement of the latter in mutant mice. This possibility is supported by at least two previous studies. In theoretical models, O'Reilly and McClelland suggested a trade-off between these two mnemonic processes (O'Reilly and McClelland, 1994). In practice, MF boutons from young and old GCs were found to share the same spines of CA3 cells in some cases but synapse separately on different spines from CA3 cells in other cases, suggesting a competition for their targets (Toni et al., 2008). Such a competition or trade-off may be subtly controlled to maintain the optimal balance of separation and completion, and the effect of the reduction of one on the other may not necessarily be revealed in all discrimination tasks. Another possibility for the lack of enhanced discrimination in the radial maze task in our mutants is that discrimination may already be saturated in control mice.

How would MFs from old GCs favor pattern completion whereas MFs from young GCs promote pattern separation? The core of our hypothesis is that old GCs may tend to lead the system into previously existing CA3 attractor states, whereas younger GCs may help form new attractor states in CA3. Old GCs are likely to have participated in the formation of many memory engrams of numerous past experiences because they have been encoding information throughout the animal's life. These engrams are likely overlapping, perhaps reflecting a high degree of engram overlap in the EC and the high redundancy of the EC→DG connections (Amaral et al., 1990). This is supported by *in vivo* physiology studies showing that it is largely the same GCs, firing at different rates, that allow the DG to generate different representations of similar but distinct environments (Leutgeb et al., 2007). In contrast, young GCs have only recently been incorporated into the functional network, and memory engrams supported by these cells would be greatly limited in their diversity and less likely to overlap than engrams supported by old GCs. When an animal encounters a new experience, both old and young GCs would participate in the formation of the new engram in the dentate. These cells would then converge downstream on CA3 to form corresponding engrams. The greater the young GCs' contribution to the dentate engram, the more distinct the new dentate and CA3 engrams would be, whereas the old GCs would have an opposite effect. In this process, the numerical disadvantage of young GCs over the old GCs may be compensated by the greater excitability and synaptic plasticity of young GCs (Schmidt-Hieber et al., 2004; Ge et al., 2007; Kee et al., 2007; Tashiro et al., 2007), and there may be additional unknown mechanisms that may favor the output of these cells (e.g., differential connection with inhibitory neurons). When two experiences are very similar, a greater participation of young GCs would be crucial for separation, whereas the discrimination of a more distinct pair of experiences

can be accomplished by greater participation of old GCs. Moreover, our data indicate that for a given pair of experiences, the ability to distinguish (separate) can be improved by the repetition of the experiences, presumably via synaptic plasticity (Figures 5 and 6) (McHugh et al., 2007).

For pattern completion, information that arrives at the DG via the EC is from partial or degraded recall cues. Such information will activate the previously formed CA3 memory engram more efficiently if it can first activate overlapping DG engrams to which old GCs contributed more than young GCs. Thus, the role of old GCs in pattern completion may be to rapidly initiate the reactivation of the relevant recurrent network in CA3 that contains the engram for the episode.

Our data indicate that the recall of old memories and the formation of new memories preferentially involve two distinct anatomical substrates consisting of varying subsets of GCs of different ages in the hippocampal DG. Therefore, adult-born GCs likely have a critical period of a few weeks in which they support pattern separation, and as they age, these cells may undergo a functional switch from pattern separation to acquiring an increased ability to trigger pattern completion-mediated recall.

EXPERIMENTAL PROCEDURES

All methods and statistics are described in detail in the [Extended Experimental Procedures](#).

Generation of Mice

DG-TeTX mice and their control littermates (Tg1 × Tg3-TeTX) were generated using a strategy similar to that previously described (Nakashiba et al., 2008) combined with the POMC-Cre transgenic line (Tg1) (McHugh et al., 2007). Mice were raised with drinking water containing 10 µg/ml Dox (Sigma) supplemented with 1% sucrose (Sigma) from the time of conception to weaning and then with food containing 10 mg Dox/kg (Bioserve) from weaning to adulthood.

Histological Methods

Immunofluorescence was performed on cryosections or vibratome sections of tissue perfused with 4% paraformaldehyde following standard protocols.

In Vitro Slice Physiology

Field excitatory postsynaptic potentials (fEPSPs) were measured in 300 µm-thick hippocampal slices with MF, PP, or RC stimulation. Whole-cell patch clamp recordings were performed from young adult-born GCs in hippocampal slices of mice injected by Moloney virus.

Moloney Virus Generation and Injection

The Moloney virus was generated in transfected 293T cells following standard protocols (Lois et al., 2002). Concentrated viral aliquots (0.9 µl, approximately 10⁹ infectious units/ml) were injected into the DG at the following sites (in mm): AP = -2.06 and ML = +1.25 from bregma, DV = -1.75 from the brain surface; AP = -2.70 and ML = +2.00 from bregma, DV = -1.75 from the brain surface.

Behavioral Experiments

Hippocampal-dependent behavioral tasks included contextual discrimination (McHugh et al., 2007), eight-arm radial maze (Clelland et al., 2009), pre-exposure-dependent contextual fear conditioning (Nakashiba et al., 2008), and Morris water maze (Nakazawa et al., 2002; Slutsky et al., 2010).

In Vivo Electrophysiology

Control (n = 14) and DG-TeTX mice (n = 18) were familiarized to one of the two environments for 3 days. On testing day 4, putative neurons from the CA1 and CA3 regions of the hippocampus were recorded while animals explored the familiar environment for 15 min, followed by the presentation of the contrasting

novel environment for 15 min. Before and after each RUN session, mice were placed for 20 min in a small "SLEEP" box separate from the recording arenas. The presentation of arenas was randomized between animals.

Statistical Analysis

All data are presented as mean ± standard error of the mean (SEM). Comparisons between two-group data were analyzed by Student's t test. If the data did not meet the assumptions of the t test, the data were analyzed with the nonparametric Mann-Whitney U-test. Multiple group comparisons were assessed using a two-way or repeated-measures ANOVA, followed by the Bonferroni's post-hoc test when necessary. With Scheffé's method to correct for multiple comparisons, discrimination training was analyzed for each trial block within each genotype, with a protection significance level of p = 0.05. The null hypothesis was rejected at the p < 0.05 level.

SUPPLEMENTAL INFORMATION

Supplemental Information includes Extended Experimental Procedures, seven figures, and two tables and can be found with this article online at [doi:10.1016/j.cell.2012.01.046](https://doi.org/10.1016/j.cell.2012.01.046).

ACKNOWLEDGMENTS

We wish to thank F. Bushard, A. Ogawa, J. Derwin, C. Lovett, D. Rooney, C. Twiss, M. Pfau, and M. Serock for excellent technical assistance, Tonegawa lab members including J. Biedenkapp, J. Young, and G. Dragoi for comments on earlier versions of the manuscript, N. Arzumian for help with manuscript preparation, C. Lois for plasmids, I. Wickersham and H.S. Seung for the rabies virus, and S. Lee for help with preliminary irradiation experiments. This work was supported by the Howard Hughes Medical Institute, the Otsuka Maryland Research Institute, the Picower Foundation, and NIH grants R01-MH078821 and P50-MH58880 to S.T.; NIH grant R01-MH62122 to M.S.F.; and NICHD intramural funding to C.J.M.

Received: April 26, 2011

Revised: December 5, 2011

Accepted: January 12, 2012

Published online: February 23, 2012

REFERENCES

- Altman, J., and Bayer, S.A. (1990). Migration and distribution of two populations of hippocampal granule cell precursors during the perinatal and postnatal periods. *J. Comp. Neurol.* 307, 365–381.
- Altman, J., and Das, G.D. (1965). Autoradiographic and histological evidence of postnatal hippocampal neurogenesis in rats. *J. Comp. Neurol.* 124, 319–335.
- Amaral, D.G., Ishizuka, N., and Claiborne, B. (1990). Neurons, numbers and the hippocampal network. *Prog. Brain Res.* 83, 1–11.
- Bakker, A., Kirwan, C.B., Miller, M., and Stark, C.E.L. (2008). Pattern separation in the human hippocampal CA3 and dentate gyrus. *Science* 319, 1640–1642.
- Braz, J.M., Rico, B., and Basbaum, A.I. (2002). Transneuronal tracing of diverse CNS circuits by Cre-mediated induction of wheat germ agglutinin in transgenic mice. *Proc. Natl. Acad. Sci. USA* 99, 15148–15153.
- Burgess, N., Maguire, E.A., and O'Keefe, J. (2002). The human hippocampus and spatial and episodic memory. *Neuron* 35, 625–641.
- Clelland, C.D., Choi, M., Romberg, C., Clemenson, G.D., Jr., Fragniere, A., Tyers, P., Jessberger, S., Saksida, L.M., Barker, R.A., Gage, F.H., and Bussey, T.J. (2009). A functional role for adult hippocampal neurogenesis in spatial pattern separation. *Science* 325, 210–213.
- Creer, D.J., Romberg, C., Saksida, L.M., van Praag, H., and Bussey, T.J. (2010). Running enhances spatial pattern separation in mice. *Proc. Natl. Acad. Sci. USA* 107, 2367–2372.
- Eriksson, P.S., Perfilieva, E., Björk-Eriksson, T., Alborn, A.M., Nordborg, C., Peterson, D.A., and Gage, F.H. (1998). Neurogenesis in the adult human hippocampus. *Nat. Med.* 4, 1313–1317.

- Fanselow, M. (1986). Associative vs topographical accounts of the immediate shock-freezing deficit in rats: Implications for the response selection rules governing species-specific defensive reactions. *Learn. Motiv.* *17*, 16–39.
- Fanselow, M. (1990). Factors governing one-trial contextual conditioning. *Anim. Learn. Behav.* *18*, 264–270.
- Ge, S., Yang, C.-H., Hsu, K.-S., Ming, G.-L., and Song, H. (2007). A critical period for enhanced synaptic plasticity in newly generated neurons of the adult brain. *Neuron* *54*, 559–566.
- Gilbert, P.E., Kesner, R.P., and Lee, I. (2001). Dissociating hippocampal subregions: double dissociation between dentate gyrus and CA1. *Hippocampus* *11*, 626–636.
- Gould, E., Beylin, A., Tanapat, P., Reeves, A., and Shors, T.J. (1999). Learning enhances adult neurogenesis in the hippocampal formation. *Nat. Neurosci.* *2*, 260–265.
- Hasselmo, M.E., Schnell, E., and Barkai, E. (1995). Dynamics of learning and recall at excitatory recurrent synapses and cholinergic modulation in rat hippocampal region CA3. *J. Neurosci.* *15*, 5249–5262.
- Hunsaker, M.R., and Kesner, R.P. (2008). Evaluating the differential roles of the dorsal dentate gyrus, dorsal CA3, and dorsal CA1 during a temporal ordering for spatial locations task. *Hippocampus* *18*, 955–964.
- Imayoshi, I., Sakamoto, M., Ohtsuka, T., Takao, K., Miyakawa, T., Yamaguchi, M., Mori, K., Ikeda, T., Itohara, S., and Kageyama, R. (2008). Roles of continuous neurogenesis in the structural and functional integrity of the adult forebrain. *Nat. Neurosci.* *11*, 1153–1161.
- Jung, M.W., and McNaughton, B.L. (1993). Spatial selectivity of unit activity in the hippocampal granular layer. *Hippocampus* *3*, 165–182.
- Kee, N., Teixeira, C.M., Wang, A.H., and Frankland, P.W. (2007). Preferential incorporation of adult-generated granule cells into spatial memory networks in the dentate gyrus. *Nat. Neurosci.* *10*, 355–362.
- Kesner, R.P. (2007). A behavioral analysis of dentate gyrus function. *Prog. Brain Res.* *163*, 567–576.
- Laplagne, D.A., Espósito, M.S., Piatti, V.C., Morgenstern, N.A., Zhao, C., van Praag, H., Gage, F.H., and Schinder, A.F. (2006). Functional convergence of neurons generated in the developing and adult hippocampus. *PLoS Biol.* *4*, e409.
- Lee, I., and Kesner, R.P. (2004). Encoding versus retrieval of spatial memory: double dissociation between the dentate gyrus and the perforant path inputs into CA3 in the dorsal hippocampus. *Hippocampus* *14*, 66–76.
- Leutgeb, J.K., Leutgeb, S., Moser, M.-B., and Moser, E.I. (2007). Pattern separation in the dentate gyrus and CA3 of the hippocampus. *Science* *315*, 961–966.
- Lois, C., Hong, E.J., Pease, S., Brown, E.J., and Baltimore, D. (2002). Germline transmission and tissue-specific expression of transgenes delivered by lentiviral vectors. *Science* *295*, 868–872.
- Marr, D. (1971). Simple memory: a theory for archicortex. *Philos. Trans. R. Soc. Lond. B Biol. Sci.* *262*, 23–81.
- Matus-Amat, P., Higgins, E.A., Barrientos, R.M., and Rudy, J.W. (2004). The role of the dorsal hippocampus in the acquisition and retrieval of context memory representations. *J. Neurosci.* *24*, 2431–2439.
- McHugh, T.J., Jones, M.W., Quinn, J.J., Balthasar, N., Coppari, R., Elmquist, J.K., Lowell, B.B., Fanselow, M.S., Wilson, M.A., and Tonegawa, S. (2007). Dentate gyrus NMDA receptors mediate rapid pattern separation in the hippocampal network. *Science* *317*, 94–99.
- McNaughton, B.L., and Morris, R.G.M. (1987). Hippocampal synaptic enhancement and information storage within a distributed memory system. *Trends Neurosci.* *10*, 408–415.
- Nacher, J., Crespo, C., and McEwen, B.S. (2001). Doublecortin expression in the adult rat telencephalon. *Eur. J. Neurosci.* *14*, 629–644.
- Nakashiba, T., Young, J.Z., McHugh, T.J., Buhl, D.L., and Tonegawa, S. (2008). Transgenic inhibition of synaptic transmission reveals role of CA3 output in hippocampal learning. *Science* *319*, 1260–1264.
- Nakazawa, K., Quirk, M.C., Chitwood, R.A., Watanabe, M., Yeckel, M.F., Sun, L.D., Kato, A., Carr, C.A., Johnston, D., Wilson, M.A., and Tonegawa, S. (2002). Requirement for hippocampal CA3 NMDA receptors in associative memory recall. *Science* *297*, 211–218.
- O'Reilly, R.C., and McClelland, J.L. (1994). Hippocampal conjunctive encoding, storage, and recall: avoiding a trade-off. *Hippocampus* *4*, 661–682.
- Overstreet, L.S., Hentges, S.T., Bumashny, V.F., de Souza, F.S.J., Smart, J.L., Santangelo, A.M., Low, M.J., Westbrook, G.L., and Rubinstein, M. (2004). A transgenic marker for newly born granule cells in dentate gyrus. *J. Neurosci.* *24*, 3251–3259.
- Sahay, A., Scobie, K.N., Hill, A.S., O'Carroll, C.M., Kheirbek, M.A., Burghardt, N.S., Fenton, A.A., Dranovsky, A., and Hen, R. (2011). Increasing adult hippocampal neurogenesis is sufficient to improve pattern separation. *Nature* *472*, 466–470.
- Santarelli, L., Saxe, M., Gross, C., Surget, A., Battaglia, F., Dulawa, S., Weisstaub, N., Lee, J., Duman, R., Arancio, O., et al. (2003). Requirement of hippocampal neurogenesis for the behavioral effects of antidepressants. *Science* *301*, 805–809.
- Schlessinger, A.R., Cowan, W.M., and Gottlieb, D.I. (1975). An autoradiographic study of the time of origin and the pattern of granule cell migration in the dentate gyrus of the rat. *J. Comp. Neurol.* *159*, 149–175.
- Schmidt-Hieber, C., Jonas, P., and Bischofberger, J. (2004). Enhanced synaptic plasticity in newly generated granule cells of the adult hippocampus. *Nature* *429*, 184–187.
- Scobie, K.N., Hall, B.J., Wilke, S.A., Klemenhagen, K.C., Fujii-Kuriyama, Y., Ghosh, A., Hen, R., and Sahay, A. (2009). Krüppel-like factor 9 is necessary for late-phase neuronal maturation in the developing dentate gyrus and during adult hippocampal neurogenesis. *J. Neurosci.* *29*, 9875–9887.
- Scoville, W.B., and Milner, B. (1957). Loss of recent memory after bilateral hippocampal lesions. *J. Neurol. Neurosurg. Psychiatry* *20*, 11–21.
- Slutsky, I., Abumaria, N., Wu, L.-J., Huang, C., Zhang, L., Li, B., Zhao, X., Govindarajan, A., Zhao, M.-G., Zhuo, M., et al. (2010). Enhancement of learning and memory by elevating brain magnesium. *Neuron* *65*, 165–177.
- Snyder, J.S., Choe, J.S., Clifford, M.A., Jeurling, S.I., Hurley, P., Brown, A., Kamhi, J.F., and Cameron, H.A. (2009). Adult-born hippocampal neurons are more numerous, faster maturing, and more involved in behavior in rats than in mice. *J. Neurosci.* *29*, 14484–14495.
- Squire, L.R., Stark, C.E.L., and Clark, R.E. (2004). The medial temporal lobe. *Annu. Rev. Neurosci.* *27*, 279–306.
- Tabuchi, K., Sawamoto, K., Suzuki, E., Ozaki, K., Sone, M., Hama, C., Tanifuji-Morimoto, T., Yuasa, Y., Yoshihara, Y., Nose, A., and Okano, H. (2000). GAL4/UAS-WGA system as a powerful tool for tracing *Drosophila* transsynaptic neural pathways. *J. Neurosci. Res.* *59*, 94–99.
- Tashiro, A., Makino, H., and Gage, F.H. (2007). Experience-specific functional modification of the dentate gyrus through adult neurogenesis: a critical period during an immature stage. *J. Neurosci.* *27*, 3252–3259.
- Toni, N., Laplagne, D.A., Zhao, C., Lombardi, G., Ribak, C.E., Gage, F.H., and Schinder, A.F. (2008). Neurons born in the adult dentate gyrus form functional synapses with target cells. *Nat. Neurosci.* *11*, 901–907.
- Treves, A., and Rolls, E.T. (1994). Computational analysis of the role of the hippocampus in memory. *Hippocampus* *4*, 374–391.
- Tronel, S., Belnoue, L., Grosjean, N., Revest, J.-M., Piazza, P.-V., Koehl, M., and Arous, D.N. (2012). Adult-born neurons are necessary for extended contextual discrimination. *Hippocampus* *22*, 292–298. Published online November 3 2010. 10.1002/hipo.20895.
- van Praag, H., Schinder, A.F., Christie, B.R., Toni, N., Palmer, T.D., and Gage, F.H. (2002). Functional neurogenesis in the adult hippocampus. *Nature* *415*, 1030–1034.
- Weisskopf, M.G., Castillo, P.E., Zalutsky, R.A., and Nicoll, R.A. (1994). Mediation of hippocampal mossy fiber long-term potentiation by cyclic AMP. *Science* *265*, 1878–1882.
- Wickersham, I.R., Lyon, D.C., Barnard, R.J.O., Mori, T., Finke, S., Conzelmann, K.-K., Young, J.A.T., and Callaway, E.M. (2007). Monosynaptic restriction of transsynaptic tracing from single, genetically targeted neurons. *Neuron* *53*, 639–647.

EXTENDED EXPERIMENTAL PROCEDURES

All procedures relating to animal care and treatment conformed to Institutional and NIH guidelines. All behavioral experiments were conducted by operators blind to genotype and Dox treatment.

Generation of Mice

α CamKII-loxP-STOP-loxP-tTA (Tg2) and TetO-TeTX (Tg3-TeTX) transgenic mice were generated in the same manner as previously described (Nakashiba et al., 2008) and maintained in a C57BL/6 genetic background. We selected different Tg2 and Tg3-TeTX transgenic lines (Tg2 line 2 and Tg3-TeTX line 2) from those used in CA3-TeTX mice (Nakashiba et al., 2008) due to difficulties in efficiently obtaining triple-transgenic DG-TeTX mice. The POMC-Cre transgenic line is the same as previously described (McHugh et al., 2007). To obtain DG-TeTX mice, heterozygous Tg1 \times Tg3-TeTX (*POMC-Cre*+/+, *TetO-TeTX line 2*/+) mice were crossed to generate homozygous double-transgenic mice (*POMC-Cre/POMC-Cre, TetO-TeTX line 2/TetO-TeTX line 2*). Male homozygous mice were then bred with the female Tg2 line 2 (α CamKII-loxP-STOP-loxP-tTA line 2/+). Half of the resultant progeny was thus heterozygous triple-transgenic mice (*POMC-Cre*+/+, *TetO-TeTX line 2*/+, α CamKII-loxP-STOP-loxP-tTA line 2/+), herein referred to as DG-TeTX mice. The other half of the progeny was thus heterozygous double-transgenic mice (*POMC-Cre*+/+, *TetO-TeTX line 2*/+, +/+), which did not express TeTX and therefore served as control mice. DG-GFP mice were generated in a similar manner by using Tg3-GFP mice (Nakashiba et al., 2008) instead of TetO-TeTX line 2 during the breeding procedure. In the Tg3-GFP line, a bidirectional TetO promoter (pBI from Clontech) drives *GFP* and *NR3B* genes. Tail DNA from all offspring was genotyped by PCR to detect the presence of each transgene separately. PCR primers and conditions were as previously described (Nakashiba et al., 2008).

Dox Treatment

DG-GFP mice, DG-TeTX mice, and their control littermates were raised with drinking water containing 10 μ g/ml Dox (Sigma) supplemented with 1% sucrose (Sigma) from the time of conception to weaning (3 weeks old) and then with food containing 10 mg Dox per kg (Bioserve) from weaning to adulthood. This protocol was sufficient to repress GFP expression in DG-GFP mice as assessed by immunohistochemistry with the GFP antibody (Figure 1) and TeTX expression as assessed with the VAMP2 antibody (Figure 1).

General Histology

All mice were transcardially perfused with 4% paraformaldehyde (PFA) in phosphate-buffered saline (PBS), and brains were post-fixed by the same fixative overnight. For vibratome sections, the brains were sliced (50 μ m thick) after overnight post-fixation. For cryostat sections, the brains were further processed in 30% sucrose, embedded in OCT compound (SAKURA), and frozen on dry ice before slicing (50 μ m thick). For GFP/Prox-1/NeuN triple staining, cryostat sections were first blocked with TNB (TSA System, PerkinElmer) containing 3% normal goat serum for 30 min and incubated with primary antibodies (rat anti-GFP, 1/500, Nacalai USA; rabbit anti-Prox 1, 1/400, Millipore and mouse anti-NeuN, 1/100, Millipore) diluted in the same blocking solution at 4°C overnight. After rinsing sections with TNT (100 mM Tris-HCl, 150 mM NaCl, and 0.3% Triton X-100), sections were incubated with secondary antibody solution (Alexa 488-conjugated anti-rat IgG, Alexa 568-conjugated anti-rabbit IgG and Alexa 647-conjugated anti-mouse IgG; all were diluted 1/200 with TNB containing 3% normal goat serum) for 2 hr at room temperature. The sections were then rinsed with PBS, incubated with DAPI (Invitrogen), and mounted on glass slides.

For GFP/DCX/NeuN triple staining, vibratome sections were treated in the same manner as above, except goat anti-DCX (1/250, Santa Cruz Biotechnology) and normal donkey serum were used in place of anti-Prox1 and normal goat serum, respectively. DCX was visualized with Alexa 568-conjugated anti-goat IgG (1/200, Invitrogen). For VAMP2 staining, vibratome sections were first incubated with rabbit anti-VAMP2 (1/250, Synaptic Systems) primary antibody and then with Alexa 568-conjugated anti-rabbit IgG (1/200, Invitrogen) secondary antibody. For VGLUT1 staining, vibratome sections were first incubated with guinea pig anti-VGLUT1 (1/1000, Millipore) primary antibody and then with Alexa 488-conjugated anti-guinea pig IgG (1/200, Invitrogen) secondary antibody. For TUNEL staining, the in situ cell detection kit (Roche) was used following the manufacturer's instructions. As a positive control for DNA fragmentation, some sections were treated with 10 units/ml DNase I (Promega) for 1 hr prior to TUNEL staining. Images were taken with a SPOT camera (Nikon) or with confocal microscopy (Leica Microsystems, TC2-SP2 AOBIS).

In Vitro Slice Physiology

Hippocampal slices (300 μ m thick) were prepared from 3- to 6-month-old DG-TeTX mice and their control littermates. Initially, to characterize the activated (Dox-on-off) DG-TeTX mice, one activated DG-TeTX mouse and one control littermate were dissected sequentially each day, and recordings from slices obtained from both mice were interleaved with the experimenter blind to the genotype. Recordings for repressed DG-TeTX mice and re-repressed DG-TeTX mice were subsequently carried out in parallel. All mice were anesthetized with isoflurane, and brains were dissected in partial sucrose artificial cerebrospinal fluid (ACSF) containing (in mM): 80 NaCl, 3.5 KCl, 1.25 H₂PO₄, 25 NaHCO₃, 4.5 MgSO₄, 0.5 CaCl₂, 10 glucose, and 90 sucrose, equilibrated with 95% O₂ and 5% CO₂. The brains were hemisected, and transverse slices were cut using a VT-1000S vibratome (Leica Microsystems). The slices were then incubated in the above solution at 35°C for 30 min and then kept at room temperature in the same solution until use.

For recordings, slices were transferred to a recording chamber and perfused (3–5 ml/min, 32°C–35°C) with ACSF composed of (in mM): 130 NaCl, 24 NaHCO₃, 3.5 KCl, 1.25 NaH₂PO₄, 2.5 CaCl₂, 1.5 MgCl₂, 10 glucose, 0.05 \pm dl-AP5 and 0.01 bicuculline

methobromide, saturated with 95% O₂ and 5% CO₂, pH 7.4. fEPSPs were recorded using electrodes (2–3 M Ω) pulled from borosilicate glass (World Precision Instruments) filled with oxygenated ACSF and connected to a multiclamp 700A amplifier (Axon Instruments, Foster City, CA, USA). For MF \rightarrow CA3 fEPSPs, the recording electrode was placed in the s. lucidum, whereas the recording electrode was placed in CA3 s. radiatum to record PP \rightarrow CA3 and RC \rightarrow CA3 fEPSPs. Synaptic responses were evoked at 0.1 Hz by stimulation (150 μ s duration, 0.05 to 0.25 mA intensity) via a constant current isolation unit (A360, World Precision Instruments, Sarasota, FL, USA) connected to glass electrode filled with oxygenated ACSF placed in the DG cell layer, the lateral PP or the CA3 s. radiatum to stimulate MF, PP, and RC inputs, respectively. Data acquisition (filtered at 3 kHz and digitized at 20 kHz) and analysis were performed using a PC equipped with pClamp 9.2 software (Axon Instruments).

Input-output (I-O) relations for each pathway were obtained by stepping the stimulus intensity from 0.05 mA to 0.25 mA. For MF \rightarrow CA3 recordings, an I/O relation was obtained in control or forskolin (20 μ M, Sigma)-supplemented ACSF and then again in the presence of DCGIV (2 μ M, Tocris). Averaged waveforms (10 consecutive sweeps) obtained in DCGIV at each stimulus intensity were digitally subtracted from the corresponding averaged waveform (i.e., same intensity) obtained in control ACSF or forskolin to obtain pure MF \rightarrow CA3 fEPSPs (Kamiya et al., 1996). For analysis, the area of the pure MF \rightarrow CA3 fEPSPs was determined in the first 2.5 ms after the end of the AFV determined prior to the digital subtraction. Area was used rather than peak or slope because MF fEPSPs have complicated waveforms that may confound peak or slope measurements, particularly in the activated DG-TeTX mice (e.g., see waveforms in Figures 2A and 2B). AFV amplitude for MF \rightarrow CA3 recordings was measured directly from non-DCGIV-subtracted traces. For PP \rightarrow CA3 and RC \rightarrow CA3 recordings, the AFV and fEPSP peaks were measured directly from averaged waveforms (minimum of 10 consecutive) obtained at each stimulus intensity.

To characterize the electrophysiological properties of adult-born GCs, slices were prepared from mice 3–4 weeks after injection of Moloney virus encoding GFP. GFP-expressing GCs were then targeted for whole-cell patch clamp recording. Slices were perfused (3–5 ml/min) with extracellular solution composed of (in mM) 130 NaCl, 24 NaHCO₃, 3.5 KCl, 1.25 NaH₂PO₄, 2.5 CaCl₂, 1.5 MgCl₂, and 10 glucose, saturated with 95% O₂ and 5% CO₂ (pH 7.4). Recordings were performed at 32°C–34°C with electrodes (3–5 M Ω) pulled from borosilicate glass (World precision instruments) filled with either (in mM) 150 K-gluconate, 3 MgCl₂, 0.5 EGTA, 2 MgATP, 0.3 Na₂GTP, and 10 HEPES plus 2 mg/ml biocytin for characterization of membrane properties and LTP experiments or 130 CsCl, 8.5 NaCl, 0.5 EGTA, 4 MgATP, 0.5 Na₂GTP, 5 QX-314Cl, and 10 HEPES for basic postsynaptic current (excitatory and inhibitory) characterization. Whole-cell patch clamp recordings were made using a Multiclamp 700A or 700B amplifier (Molecular Devices, Sunnyvale, CA, USA) in current- or voltage clamp-mode. The signals were filtered at 3 kHz (Bessel filter; Frequency Devices, Haverhill, MA, USA) and digitized at 20 kHz (Digidata 1322A or 1440A and pClamp 9.2 or 10.2 Software; Molecular Devices). Recordings were not corrected for a liquid junction potential.

The resting membrane potential was noted immediately upon achieving a whole-cell configuration. The membrane potential was then biased to –60 mV by constant current injection. The input resistance (R_m) was measured using a linear regression of voltage deflections (\pm 15 mV from the resting potential, \sim 60 mV) in response to 2 s current steps of 6–10 different amplitudes in 5 pA steps. The membrane time constant (τ_m) was calculated from the mean responses to 20 successive hyperpolarizing current pulses (–20 pA; 400 ms) and was determined by fitting voltage responses with a single exponential function. Action potential (AP) threshold was defined as the voltage at which the slope trajectory reached 10 mV/ms (Stuart and Häusser, 1994) and AP amplitude was defined as the difference in membrane potential between the threshold and the peak. Spike half-width was defined as the duration of the AP at half of the determined amplitude. These properties were measured for the first two action potentials elicited by a depolarizing 800 ms current pulse of amplitude that was just sufficient to bring the cell to threshold for AP generation. Firing frequency was calculated from the number of spikes observed during the 800 ms window during a current injection twice this amount. All intrinsic electrophysiological parameters were measured in pClamp or using procedures written in Igor 6 (Wavemetrics, Portland, OR, USA).

Spontaneous inhibitory postsynaptic currents (sIPSCs) were pharmacologically isolated by the addition of DNQX (10 μ M) and dl-AP5 (50 μ M) to the perfusing medium and recorded as inward currents at a holding potential of –70 mV with the chloride reversal potential set to 0 mV (CsCl based internal). Events were detected using a template matching algorithm and analyzed in pClamp. At the end of the recordings, bicuculline (10 μ M) was added to the perfusing medium to determine the tonic GABAergic current. Spontaneous and evoked excitatory postsynaptic currents (s/eEPSCs) were pharmacologically isolated by the addition of bicuculline to the perfusing medium. sEPSCs were recorded at a holding potential of –70 mV and detected by a template matching strategy and analyzed in pClamp. eEPSCs were elicited at 0.1 Hz as paired pulses (20 Hz) by low-intensity microstimulation (100 μ s duration; 10–30 μ A intensity) via a constant-current isolation unit (A360, World Precision Instruments) connected to a patch electrode filled with oxygenated extracellular solution placed in the molecular layer. The AMPA receptor-mediated component was determined from the peak of the eEPSC (the first event of paired pulses) observed at a holding potential of –70 mV, and the NMDA receptor-mediated component was measured 25 ms after the peak at a holding potential of +40 mV. Paired pulse ratios (PPRs) were calculated as the mean P2/mean P1, where P1 was the amplitude of the first evoked current and P2 was the amplitude of the second synaptic current obtained for consecutive individual traces.

For LTP experiments, bicuculline was added to the perfusing medium, and AMPAR-mediated EPSCs were monitored in voltage clamp mode (V_h = –70mV) before (2–3 min) and after (15–20 min) LTP induction with a theta burst stimulation (TBS) protocol (Schmidt-Hieber et al., 2004). TBS was performed in current clamp mode with the membrane potential biased to –60 mV via constant current injection. TBS consisted of 10 trains of stimuli at 5 Hz, with each train consisting of 10 stimuli at 100 Hz. The duration of each train was paired with a postsynaptic depolarizing current injection of 300–400 pA that was sufficient to evoke a burst of postsynaptic

action potentials. This was repeated four times at a frequency of 0.1 Hz, after which the recording configuration was switched back to voltage clamp mode, and AMPAR-mediated EPSCs were monitored as described above for a minimum of 20 min post-TBS.

BrdU Injection and Histology

For BrdU experiments to characterize adult neurogenesis, 14- to 20-week-old DG-TeTX and their control littermates received four injections of BrdU (75 mg/kg body weight per injection, Sigma) separated by 2 hr. The mice were then sacrificed at the time points indicated in Figure S3. Cryostat sections (50 μ m thick) were first treated with 2N HCl in PBS containing 0.1% Triton X-100 (PBST-0.1%) for 30 min at 37°C. After washing with PBS three times, the sections were blocked and incubated with primary antibodies (rat anti-BrdU, 1/100, Accurate Chemical; mouse anti-NeuN, 1/100, Millipore; rabbit anti-GFAP, 1/500, Dako) in PBST-0.1% containing 3% normal goat serum at 4°C overnight. The sections were then rinsed with PBS and incubated with secondary antibodies (Alexa 488-conjugated anti-mouse IgG, Alexa 568-conjugated anti-rat IgG and Alexa 633-conjugated anti-rabbit IgG, all diluted 1/200, Invitrogen) in PBS for 2 hr at room temperature. The number of BrdU-positive cells ($n = 8$ –10 mice per genotype/condition) was counted in every sixth section throughout the entire extent of the DG.

Virus Generation, Injection, and Histological Characterization

We used a Moloney viral vector (Molar, a kind gift from Dr. Carlos Lois) containing an internal promoter derived from the Rous sarcoma virus. Viral vectors were modified as follows. For coexpression of SypGFP and mCherry-VAMP2 fusion proteins, mCherry was fused in frame to the cDNA of VAMP2 by PCR to generate mCherry-VAMP2. This was subcloned downstream from the encephalomyelocarditis virus internal ribosomal entry site (IRES) to generate IRES-mCherry-VAMP2, which was then subcloned downstream from SypGFP cDNA (from Dr. Carlos Lois). The resultant bicistronic SypGFP-IRES-mCherry-VAMP2 was then cloned under the promoter in the Molar vector. For expression of wheat germ agglutinin (WGA) in a Cre-dependent manner, a DNA cassette carrying two pairs of incompatible lox sites (loxP and lox2272) was synthesized, and the WGA cDNA (Addgene) was inserted between loxP and lox2272 sites in the reverse orientation. The resulting double-floxed reverse WGA cassette was cloned downstream from the promoter in the Molar vector. WGA cDNA was generated by PCR with 15 amino acids deleted at the C terminus (Yoshihara et al., 1999). The viral vector for the expression of GFP in a Cre-dependent manner was generated in an identical manner to the WGA vector. A viral vector for Cre-independent mCherry expression was obtained from Dr. Carlos Lois.

We examined which neurons made direct synaptic contact to young, adult-born GCs using rabies monosynaptic retrograde labeling from defined cells (Wickersham et al., 2007). This virus can retrogradely cross synapses through the rabies envelope protein (G). The rabies virus was modified to replace the rabies G gene with a fluorescent marker and thus became incompetent for retrograde labeling unless rabies G is provided in infected cells. To restrict rabies viral infection to a desired population of cells, the rabies virus was further pseudotyped with EnvA, an avian viral envelope protein, whose receptors mammals lack. This modified rabies virus (EnvA Δ G) can infect cells expressing the EnvA receptor TVA. If TVA-expressing cells also express rabies G, the EnvA Δ G virus can utilize the cell-provided rabies G protein and thus be transferred to the presynaptic cells in a retrograde manner. However, the transfer is limited to monosynaptic connections, as *trans*-synaptically infected cells do not express the rabies G protein. In order to express TVA and rabies G glycoprotein in young, adult-born GCs, a Cre-dependent Moloney virus was generated. A double-floxed DNA cassette containing *GFP*, *TVA*, and rabies G glycoprotein fused with 2A signals was obtained from Addgene (Wall et al., 2010) and cloned downstream from the promoter in the Molar vector in the reverse orientation.

Moloney viral particles were produced via calcium phosphate cotransfection of 293T cells with the viral vectors, Eco, and VSV (from Dr. Carlos Lois) in the same procedure as previously described (Lois et al., 2002). Supernatants were collected starting from 36 hr after the transfection for 36 hr and concentrated by ultracentrifugation at 25,000 rpm for 90 min. The resulting viral pellet was resuspended in PBS at 1/500th of the original volume, and the viral aliquot was then frozen. Viral titers were approximately 10⁹ infectious units/ml. DG-TeTX mice and their control littermates (12–16 weeks old) were anesthetized with avertin and stereotaxically injected at two sites targeting the right DG (0.9 μ l of viral aliquot per site). The stereotaxic coordinate for the first site was 2.06 mm posterior from bregma, 1.25 mm lateral from the midline and 1.75 mm ventral from the brain surface. The second site was 2.70 mm posterior from bregma, 2.00 mm lateral from the midline and 1.75 mm ventral from the brain surface. The scalp incision was sutured, and post-injection analgesics were given to aid recovery (0.1 mg/kg, buprenex). For the viral coinjection described in Figure S4, equal amounts of the Cre-dependent GFP virus and the Cre-independent mCherry virus were mixed, and 0.9 μ l of the viral mixture was injected at the same location as above. For rabies monosynaptic retrograde labeling, a Cre-dependent Moloney virus encoding GFP, TVA, and rabies G glycoprotein was first injected into the DG at the same sites as above (0.9 μ l of viral aliquot per site). Three weeks later, the EnvA-pseudotyped and G-deleted rabies virus containing RFP (9.3×10^8 infectious units/ml) was injected at the same sites (0.45 μ l of viral aliquot per site).

At the time points after virus injection indicated in the figures, all mice were transcardially perfused with 4% PFA in PBS and brains were post-fixed by the same fixative overnight. Brain sections were prepared in the same manner described above. For double immunostaining for GFP and mCherry, vibratome sections (50 μ m thick) were used with rat anti-GFP (1/500, Nacalai USA) and rabbit anti-RFP (1/500, Rockland immunochemicals) primary antibodies and Alexa 488-conjugated anti-rat IgG (1/200, Invitrogen) and Alexa 568-conjugated anti-rabbit IgG (1/200, Invitrogen) secondary antibodies. Although the transgene construct for the Tg3-TeTX was initially generated as a fusion protein with GFP, we failed to detect any GFP-TeTX fusion protein in the DG-TeTX mice with this immunostaining procedure (data not shown). Therefore, we concluded that signals detected with this procedure were

derived solely from synaptophysin-GFP fusion proteins. For WGA and NeuN double staining, immunostaining for WGA was first performed. Cryostat sections (50 μ m thick) were treated with 3% H₂O₂ in PBS for 15 min, followed by treatment with 3% normal horse serum (NHS) in PBS containing 0.2% Triton X-100 (PBST-0.2%) for 30 min. After rinsing twice with PBS, the sections were treated with the Avidin/Biotin blocking kit (Vector laboratories) following the manufacturer's instructions. The sections were then incubated with goat anti-WGA (1/3000, Vector Laboratories) in PBST-0.2% containing 3% NHS for 2 hr at room temperature. After rinsing three times with PBST-0.2%, the sections were incubated with biotinylated anti-goat IgG (1/1000, Vector Laboratories) for 1 hr at room temperature. Next, the sections were rinsed once with PBST-0.2% and twice with PBS before incubation with streptavidin-biotin/horseradish peroxidase complex (ABC, 1/200, Vector Laboratories) for 30 min. After rinsing three times with PBS, the sections were incubated with Biotin-tyramide (1/50, PerkinElmer) at room temperature for 10 min. Following a subsequent wash with PBS three times, the sections were incubated with ABC again for 30 min and then rinsed three times with PBS. WGA signals were visualized with Cy3-tyramide (1/200, PerkinElmer) by 10 min of incubation at room temperature. The sections were then further processed for NeuN staining. After blocking with PBST-0.1% containing 3% normal donkey serum, the sections were incubated with mouse anti-NeuN (1/100, Millipore) and visualized with Alexa 488-conjugated anti-mouse IgG (1/200, Invitrogen). Finally, the sections were incubated with DAPI (Invitrogen) and mounted on glass slides. WGA signal was not observed when the virus was injected to non-Cre transgenic mice (data not shown). For rabies viral experiments, the primary antibodies used were rat anti-GFP (1/500, Nacalai USA), rabbit anti-tRFP (1/10000, Evrogen) and anti-NeuN (1/100, Millipore). Images were captured with a SPOT camera (Nikon) or with confocal microscopy (Leica Microsystems, TC2-SP2 AOBs).

Contextual Discrimination Fear Conditioning between Contexts

Fear conditioning was performed with male mice between 14 and 22 weeks of age during the light cycle in the animal facility. Activated DG-TeTX mice ($n = 12$) and their control littermates ($n = 12$) were assessed in a contextual discrimination fear conditioning between a pair of similar contexts. This procedure was based on that described previously (McHugh et al., 2007). Mice were trained to discriminate between two contexts through repeated experience in each context. The same four identical conditioning chambers (30 \times 25 \times 25 cm; Med-Associates, Inc.) were used for both context A (the context paired with a shock) and context B (never paired with a shock). The conditioning chambers were placed in a sound-attenuating cubicle with a 60 dB background noise provided by a fan. The floor of each chamber was made of 32 stainless steel rods (2 mm diameter) spaced 6 mm apart with alternating heights (4 mm offset) wired to a shock generator and scrambler (Med-Associates, Inc.) to deliver the footshock. Each chamber was wiped down with 70% ethanol before conditioning and between animals. A metal pan containing a thin film of Windex was placed underneath the grid floors and was replaced between animals. The only feature that differentiated the two contexts was that the A context had a plastic A-frame insert (two black plastic panels joined at the top and sloping down to the side of the conditioning chamber at a 60° angle to the floor), whereas context B did not. This was done to make the discrimination as difficult as possible so that the pattern separation function of the DG could be assessed. On each conditioning day, animals were brought to a holding room in their home cages and left undisturbed for a minimum of 30 min. Animals were then transported from the holding room to the conditioning chambers in their home cages.

Contextual Fear Acquisition

Animals received context conditioning on days 1 through 3. Animals were placed in context A for 3 min and allowed to explore. A 2 s 0.65 mA shock was then presented, and the animals were removed 1 min later. Freezing was measured during the 3 min preceding the shock.

Generalization Test

On day 4, animals were placed in context A or B for 3 min and then placed in the opposite context for 3 min 1.5–2 hr later, with the order counterbalanced such that half of the animals were placed in context A first and half were placed in context B first. Day 5 followed this same procedure with the order reversed. No shock was delivered in A or B during the generalization test. Freezing was measured during the 3 min.

Discrimination Training

Days 6–17 consisted of discrimination training in which animals were placed in both contexts on each day. Context A was again paired with a shock, but context B was not. The animals were placed in each context for a total of 4 min and 2 s. In context A, the animals received a 2 s 0.65 mA shock after 3 min and were left in the chamber for 1 min following the shock. In context B, the animals were placed in the chamber for an equivalent 4 min and 2 s. Freezing was measured during the 3 min preceding the shock on all days in which the shock was administered in context A and the equivalent period of time in context B during discrimination training. Freezing was measured using Video Freeze software (Med-Associates, Inc.) recorded at 30 frames per second with the freezing threshold set at 19 and the minimum freeze duration set at 1 s. The order of training followed a double alternation schedule: day 6, B \rightarrow A; day 7, A \rightarrow B; day 8, A \rightarrow B; day 9 B \rightarrow A; etc. For statistical analysis and graphical presentation, the data were collapsed into consecutive 2 day blocks so that each block consisted of one day of A \rightarrow B and one day of B \rightarrow A. Discrimination training was analyzed in a manner that allowed us to conservatively state when a group differentiated between A and B. For each trial block within each genotype using Scheffé's method to correct for multiple comparisons, with a protection significance level of $p = 0.05$. We chose the Scheffé method because we had no a priori prediction about when discrimination would emerge, and Scheffé's method retains a 0.05 confidence level regardless of the number of comparisons that are made. Only trial blocks with an effect of context that exceeded this correction were considered significant.

Contextual discrimination between a pair of very distinct contexts was performed using the same experimental schedule for the first 5 days as the one described above with activated DG-TeTX mice ($n = 12$) and their control littermates ($n = 12$) between 14 and 22 weeks of age. The chambers (context A), measuring $30 \times 25 \times 21$ cm, had plexiglass fronts and backs and were located in one room lit with overhead fluorescent lamps. The chamber floors consisted of 36 stainless steel rods placed at the same height and spaced 7.9 mm apart. The chambers were cleaned prior to an introduction of an individual mouse with 70% alcohol, and a solution of 0.25% benzaldehyde (in 100% ethanol) was placed beneath the chambers during the experiment to provide a dominant odor. The chambers (context D) had the same dimension as context A but were located in another room adjacent to the first one, which was lit with dim red light. In addition, the chambers had a curved plastic roof, and the floor consisted of 19 stainless steel rods spaced 16 mm apart with alternating heights. The chambers were cleaned with quatricide prior to the introduction of each mouse, and a solution of 1% acetic acid was placed beneath the chambers during the experiment to provide a dominant odor. The lighting, chamber materials and odor employed in context D provided a context that was quite distinct from context A.

In Figures 5H–5O, irradiation was performed with male mice between 9 and 12 weeks of age. Repressed DG-TeTX mice ($n = 28$) and their control littermates ($n = 28$) were anesthetized with a mixture of 100 mg/kg ketamine and 7 mg/kg xylazine. Half of the mice were focally irradiated by X-ray, and the other half were sham-operated (i.e., they were anesthetized but not subjected to irradiation). The mice were irradiated with three fractions of 5 Gy/day on days 1, 3, and 5 for a total dose of 15 Gy using a Gulmay Medical RS320 Irradiation System X-ray unit at 300kV (Gulmay Medical Ltd., Camberly, Surrey, UK). The beam was filtered using 1.5 mm Cu and 3 mm Al giving a HVL of 3 mm Cu at a dose rate of 1.975 Gy/min. Multiple experiments using Harshaw TLD-100H (LiF:Mg, Cu, P) and film (GAFCHROMIC EBT2, International Specialty Products, Wayne, NJ, USA) dosimetry were performed and calibrated against a clinical cobalt-60 irradiator (Theratron-1000, MDS Nordion, Ontario) indicating an inhomogeneity of the radiation doses within the field was less than 6.5%. As previously described (Santarelli et al., 2003), the mice were placed on the stereotaxic frame and protected from X-ray with a lead shield covering the entire body except the area above the hippocampus (interaural -2.64 mm to $+0.58$ mm). After irradiation, the Dox diet was replaced with a regular diet. Six weeks later, the mice were subjected to the same contextual discrimination fear conditioning as above using a different context pair (A and C). There were three different features (odor, background noise, and interior) that differentiated these contexts. The context A had background fan noise and was scented with Windex, whereas the context C did not have background noise and was scented with Simple Green. In addition, a plastic A-frame insert was placed in context C. After the completion of discrimination training, half of the mice received BrdU injections twice (75 mg/kg body weight). The mice were then transcardially perfused with 4% PFA in PBS on the following day. BrdU-positive cells in the DG were counted in the same manner as described above, and BrdU-positive cells in the subventricular zone were counted in the lateral walls of the lateral ventricle between $+1.70$ and -0.10 from bregma.

Delayed Nonmatching to Place Task in an Eight-Arm Radial Maze

The DNMP task in an eight-arm radial maze was performed in activated DG-TeTX mice ($n = 12$) and their control littermates ($n = 12$) between 14 and 22 weeks of age during the light cycle. The mice were transported from the colony to a holding room adjacent to the behavioral suite containing the eight-arm radial maze, where they sat undisturbed in their home cages for 30 min prior to the experiment. All mice were food restricted for 1 week prior to subjecting them to the task and maintained at 85% body weight throughout the experiment. Water was supplied ad libitum. After reaching the criteria, the mice were habituated to an eight-arm radial maze (Harvard Apparatus) for 2 days by allowing them to explore the maze foraging for food pellets. On the first day, mice from the same cage (two to four mice) explored the maze together for 1 hr. On the second day, they explored the maze separately for approximately 5 min. On the following day, the mice were subjected to the DNMP task, four trials per day, for 12 consecutive days. Each trial consisted of a sampling phase and a choice phase and was separated by at least 2 hr between trials. In the sample phase, the mice were placed in a start arm of the maze, in which doors for the start arm and a sample arm (rewarded) were open. After retrieving food pellets in the sample arm, the mice were returned to the home cage and kept there for 20 s. During this 20 s period, the maze was cleaned with quatricide and set up for the choice phase, in which doors for the start arm and the sample arm (nonrewarded) and a third correct arm (rewarded) were open. The mice returned to the maze 20 s after the completion of the sample phase and were allowed to retrieve the food pellets. Mice that visited the correct arm (rewarded) were considered to have made correct choices, whereas mice that visited the sample arm (nonrewarded) were considered to have made incorrect choices and were allowed to visit the correct arm to retrieve the food pellets before being returned to the home cage. The correct arms were separated from the sample arm by 45° , 90° , 135° , and 180° . The mice were subjected to four trials per day, receiving at least one trial from each separation degree every day in a pseudorandom manner. The start arm location for each trial was also determined in a pseudorandom manner.

Pre-exposure-Mediated Contextual Fear Conditioning

Pre-exposure-mediated contextual fear conditioning was conducted with male mice between 14 to 22 weeks of age during the light cycle. The mice were transported from the colony to a holding room, where they sat undisturbed for 30 min prior to the experiment. The conditioning chamber (A), measuring $30 \times 25 \times 21$ cm, had plexiglass fronts and backs and were located in a room lit with dim red light. The chambers had a curved plastic roof, and the floor consisted of 19 stainless steel rods spaced 16 mm apart with alternating heights. The chambers were cleaned with quatricide prior to the introduction of an individual mouse, and a solution of 1% acetic acid was placed beneath the chambers during the experiment to provide a dominant odor. Repressed mice (i.e., Dox-on) were brought into the conditioning chamber (Figures 7B, 7C, 7D, and 7F) or a very distinct chamber (D) composed of an opaque

plastic box (30 × 20 × 20 cm) without a roof (Figure 7E). The (pre-) exposure session consisted of a free exploration of the chambers for 10 min. The mice were then transported back to their home cages. Mice were given (pre-) exposure sessions for 5 consecutive days, 10 min per day, and the Dox diet was then replaced with a Dox-free diet (Figures 7B, 7C, 7E, and 7F) or unchanged (Figure 7D). Four weeks later, the mice were transported individually to the conditioning chamber and then received a single 1.5 mA footshock (2 s duration) 10 s (Figures 7B, 7D, and 7E) or 3 min (Figure 7C) after being placed in the chamber or did not receive a footshock 10 s after being placed in the chamber (Figure 7F). The mice remained in the chamber for a further 30 s and were then transported back to their home cages. On the next day, the mice were returned to the conditioning chamber for a 3 min test. During all of these sessions, the activity of the animals in the chamber was recorded using the FreezeFrame software. Freezing behavior was assessed from the video image of the mouse using the FreezeView software (Med-Associates, Inc.).

Morris Water Maze

The Morris water maze task was conducted with DG-TeTX mice ($n = 23$) and control littermates ($n = 24$) between 14 and 24 weeks of age. Repressed mice (i.e., Dox-on) were kept in a temperature-controlled room on a constant 12 hr light/dark cycle. All experiments were conducted at approximately the same time of day. The mice were transported from the colony to a holding area, where they sat undisturbed for 30 min prior to the experiment. The test was performed in a rectangular dimly lit room (340 cm × 297 cm) with a circular pool (160 cm diameter) filled with opaque water made with color paints (White 5130, Berghause; Peach 2906, Pearl Temperra) maintained at 19°C. Four large objects illuminated with floor lamps were hung on black curtains surrounding the pool as extramaze cues. A hidden circular platform (13 cm in diameter) was placed 1 cm below the water surface, and the mice were trained to find the platform with four trials per day for 12 days, with an intertrial interval of approximately 60 min. During training, the mice were released from four pseudorandomly assigned start locations (N, S, E, and W) and were allowed to swim for 90 s. If a mouse did not find the platform within 90 s, it was manually guided to the platform and allowed to rest on the platform for 15 s. A probe trial was conducted on day 13 under the full-cue condition (P1; Figure S7C). The mice were released at the center of pool and were allowed to swim for 90 s in the absence of the platform. Following the probe trial, the mice received four training trials in the presence of the platform to avoid memory extinction that may have occurred during the probe trial. The mice then underwent 5 weeks of Dox withdrawal in the colony. Subsequently, the mice received four probe trials with extramaze cue manipulations, one probe trial per day, without retraining between probe trials. For the one-cue probe trial (P2; Figure 7J), one cue located more distally from the platform was kept, and the other three cues were removed from the surrounding curtains. For the two-cue probe trial (P3; Figure 7J), one cue located close to the platform and the cue used in the one-cue probe trial remained, but the other two cues were removed from the surrounding curtains. For the no-cue probe trial (P5; Figure S7D), all four extramaze cues were removed. Data for training and probe trials were collected and analyzed with the HVS Image Water 2020 software. Escape latency and distance traveled to the hidden platform and swim speed were measured during training, and the latency to the first crossing of the phantom platform location and the amount of time mice spent during the 90 s in the circular platform surface were measured during probe trials. These data were then averaged over mice of each genotype.

In Vivo Recording

Activity of hippocampal neurons (“place cells”) depends on an animal’s location in the environment (O’Keefe and Dostrovsky, 1971), and shifting a rodent from one context to another similar but distinct context in the same room results in firing rate changes of place cells without significantly changing the firing field locations (“rate remapping”), particularly in CA3 (Leutgeb et al., 2004; Leutgeb et al., 2007). In addition, we previously showed that a deficit of CA3 rate remapping correlated with an impairment of behavioral pattern separation in mice devoid of NMDA receptors in DG GCs (McHugh et al., 2007).

Surgery

Male mice (DG-TeTX and littermate controls, 16–24 weeks of age) were implanted in the right hippocampus with a microdrive array consisting of 6–12 independently adjustable tetrodes as previously described (McHugh et al., 1996) (stereotaxic coordinates from bregma [mm]: CA1: AP 1.8, ML 1.6; CA1/CA3: AP 1.6, ML 1.4). Prior to implantation, tetrodes were coated with Dil (Invitrogen) to enable tracking of their locations. At the completion of the experiment, mice were given a lethal dose of anesthetic and a small electrical current (20–50 μ A) was run down each tetrode for 5–10 s to create a small lesion at the tip. Mice were then perfused transcardially with 4% PFA in 0.1 M sodium phosphate buffer. The brains were sectioned (50 μ m) and stained with nuclear red or neurotrace green fluorescent Nissl stain. The recording position of each tetrode was verified by examining the location of the lesion and the tracks of the electrodes under fluorescence or light microscopy.

Apparatus and Recording Protocol

All experiments were performed by researchers blind to the genotypes of the animals. Mice were familiarized to one of two arenas (a low-walled black square arena [43 cm × 43 cm × 10 cm high] with a white cue card [23 cm × 8 cm high] or a low-walled white circular arena [48 cm diameter × 10 cm high] with a black cue card [23 cm × 8 cm high]) in a free exploration task for 15 min/day for 3 consecutive days. The presentation of the black square and white circle was counterbalanced between animals. Diffuse room lighting was provided by low intensity LEDs focused onto four distal salient visual cues located on black curtains that surrounded the elevated recording arena. On day 4, the pattern separation recording sessions consisted of two “RUN” epochs (15 min each). Before and after each RUN session, the mice were placed in a small high-walled box outside of the behavioral environment for 20 min (“SLEEP” sessions). RUN1 was conducted in the familiar environment in the same room and conditions as days

1–3. For RUN2, familiar arena was replaced by the novel arena (see Figure 6D). Both environments were similar in terms of area (~1800 cm²). The presentation order of the black square and white circle did not influence the results; thus, the two recording conditions were pooled.

Unit Recording and Tracking

The position of the animals was tracked at ~30 Hz using a pair of LEDs placed on the animal's headstage. As animals explored the arenas, unit activity was amplified 5,000–30,000 times and bandpass filtered at 0.3–6 kHz. Spike waveforms above a threshold of 65 μ V were time stamped and digitized at 32 kHz. A total of 1 ms of data was stored for each waveform. A single EEG channel was sampled from each tetrode continuously at ~3 kHz.

Data Analysis

Spike sorting was performed off-line using custom clustering software, and action potentials were assigned to individual cells based on a spike's relative amplitude across the four recording wires of the tetrode as previously described (McHugh et al., 1996). Cluster boundaries were compared across run and sleep sessions to determine whether clusters were derived from the same cell or not and whether recordings were stable. Hippocampal cells and interneurons were distinguished by their firing pattern (i.e., complex spike index [CSI]), spike shape, average firing rate, and spatial firing pattern. Pyramidal cells were accepted for further analysis if the average rate was >0.2 Hz and the peak firing rate was >5 Hz in at least one run. Interneurons (mean firing rate > 5 Hz and CSI < 5% in both RUN1 and RUN2) were not included in any analysis.

To characterize the consequence of the specific blockade of the vast majority of GCs on the activity of CA3 and CA1 pyramidal cells, we measured several properties, including: (1) the mean firing rate; (2) the peak firing rate; (3) the place field size, defined as the size of the largest group of contiguous pixels with a firing rate above 20% of the peak rate (Brun et al., 2002); (4) the mean in-field firing rate, defined as the total number of spikes emitted by a cell while the mouse was in the place field divided by the total time spent in the field; and (5) spatial information, or the amount of information (in bits) conveyed about spatial location by a single action potential emitted by a single cell (Markus et al., 1994), defined as $I = \sum P_i(\lambda_i/\lambda) \log_2(\lambda_i/\lambda)$, where λ_i is the mean firing rate in each pixel, λ is the overall mean firing rate, and P_i is the probability of the animal to be in pixel i (i.e., dwelling time in each pixel/the total dwelling time).

To assess the similarity in ensemble activity between RUN1 and RUN2 (pattern separation recording session, day 4), we calculated two different rate remapping indices for each pyramidal cell meeting our minimum criteria and averaged those values for each region and genotype. First, we calculated the rate difference ([high rate-low rate]/[high rate+low rate]) (McHugh et al., 2007) as well as the rate overlap (low rate/high rate) (Leutgeb et al., 2004). The rate differences for each hippocampal region and genotype were then compared to the estimated rate difference (ERD) values expected from independent firing rates in each region. For this calculation, the rate difference was calculated between cells from RUN1 and randomly chosen cells from RUN1 or RUN2. The means from 10,000 permutations were then calculated and used to represent the ERD for each region/genotype.

SUPPLEMENTAL REFERENCES

Brun, V.H., Otnass, M.K., Molden, S., Steffenach, H.-A., Witter, M.P., Moser, M.-B., and Moser, E.I. (2002). Place cells and place recognition maintained by direct entorhinal-hippocampal circuitry. *Science* 296, 2243–2246.

Kamiya, H., Shinozaki, H., and Yamamoto, C. (1996). Activation of metabotropic glutamate receptor type 2/3 suppresses transmission at rat hippocampal mossy fibre synapses. *J. Physiol.* 493, 447–455.

Leutgeb, J.K., Leutgeb, S., Moser, M.-B., and Moser, E.I. (2007). Pattern separation in the dentate gyrus and CA3 of the hippocampus. *Science* 315, 961–966.

Leutgeb, S., Leutgeb, J.K., Treves, A., Moser, M.-B., and Moser, E.I. (2004). Distinct ensemble codes in hippocampal areas CA3 and CA1. *Science* 305, 1295–1298.

Lois, C., Hong, E.J., Pease, S., Brown, E.J., and Baltimore, D. (2002). Germline transmission and tissue-specific expression of transgenes delivered by lentiviral vectors. *Science* 295, 868–872.

Markus, E.J., Barnes, C.A., McNaughton, B.L., Gladden, V.L., and Skaggs, W.E. (1994). Spatial information content and reliability of hippocampal CA1 neurons: effects of visual input. *Hippocampus* 4, 410–421.

McHugh, T.J., Jones, M.W., Quinn, J.J., Balthasar, N., Coppari, R., Elmquist, J.K., Lowell, B.B., Fanselow, M.S., Wilson, M.A., and Tonegawa, S. (2007). Dentate gyrus NMDA receptors mediate rapid pattern separation in the hippocampal network. *Science* 317, 94–99.

McHugh, T.J., Blum, K.I., Tsien, J.Z., Tonegawa, S., and Wilson, M.A. (1996). Impaired hippocampal representation of space in CA1-specific NMDAR1 knockout mice. *Cell* 87, 1339–1349.

Nakashiba, T., Young, J.Z., McHugh, T.J., Buhl, D.L., and Tonegawa, S. (2008). Transgenic inhibition of synaptic transmission reveals role of CA3 output in hippocampal learning. *Science* 319, 1260–1264.

O'Keefe, J., and Dostrovsky, J. (1971). The hippocampus as a spatial map. Preliminary evidence from unit activity in the freely-moving rat. *Brain Res.* 34, 171–175.

Santarelli, L., Saxe, M., Gross, C., Surget, A., Battaglia, F., Dulawa, S., Weisstaub, N., Lee, J., Duman, R., Arancio, O., et al. (2003). Requirement of hippocampal neurogenesis for the behavioral effects of antidepressants. *Science* 301, 805–809.

Schmidt-Hieber, C., Jonas, P., and Bischofberger, J. (2004). Enhanced synaptic plasticity in newly generated granule cells of the adult hippocampus. *Nature* 429, 184–187.

Stuart, G., and Häusser, M. (1994). Initiation and spread of sodium action potentials in cerebellar Purkinje cells. *Neuron* 13, 703–712.

Wall, N.R., Wickersham, I.R., Cetin, A., De La Parra, M., and Callaway, E.M. (2010). Monosynaptic circuit tracing in vivo through Cre-dependent targeting and complementation of modified rabies virus. *Proc. Natl. Acad. Sci. USA* 107, 21848–21853.

Wickersham, I.R., Lyon, D.C., Barnard, R.J.O., Mori, T., Finke, S., Conzelmann, K.-K., Young, J.A.T., and Callaway, E.M. (2007). Monosynaptic restriction of transsynaptic tracing from single, genetically targeted neurons. *Neuron* 53, 639–647.

Yoshihara, Y., Mizuno, T., Nakahira, M., Kawasaki, M., Watanabe, Y., Kagamiyama, H., Jishage, K., Ueda, O., Suzuki, H., Tabuchi, K., et al. (1999). A genetic approach to visualization of multisynaptic neural pathways using plant lectin transgene. *Neuron* 22, 33–41.

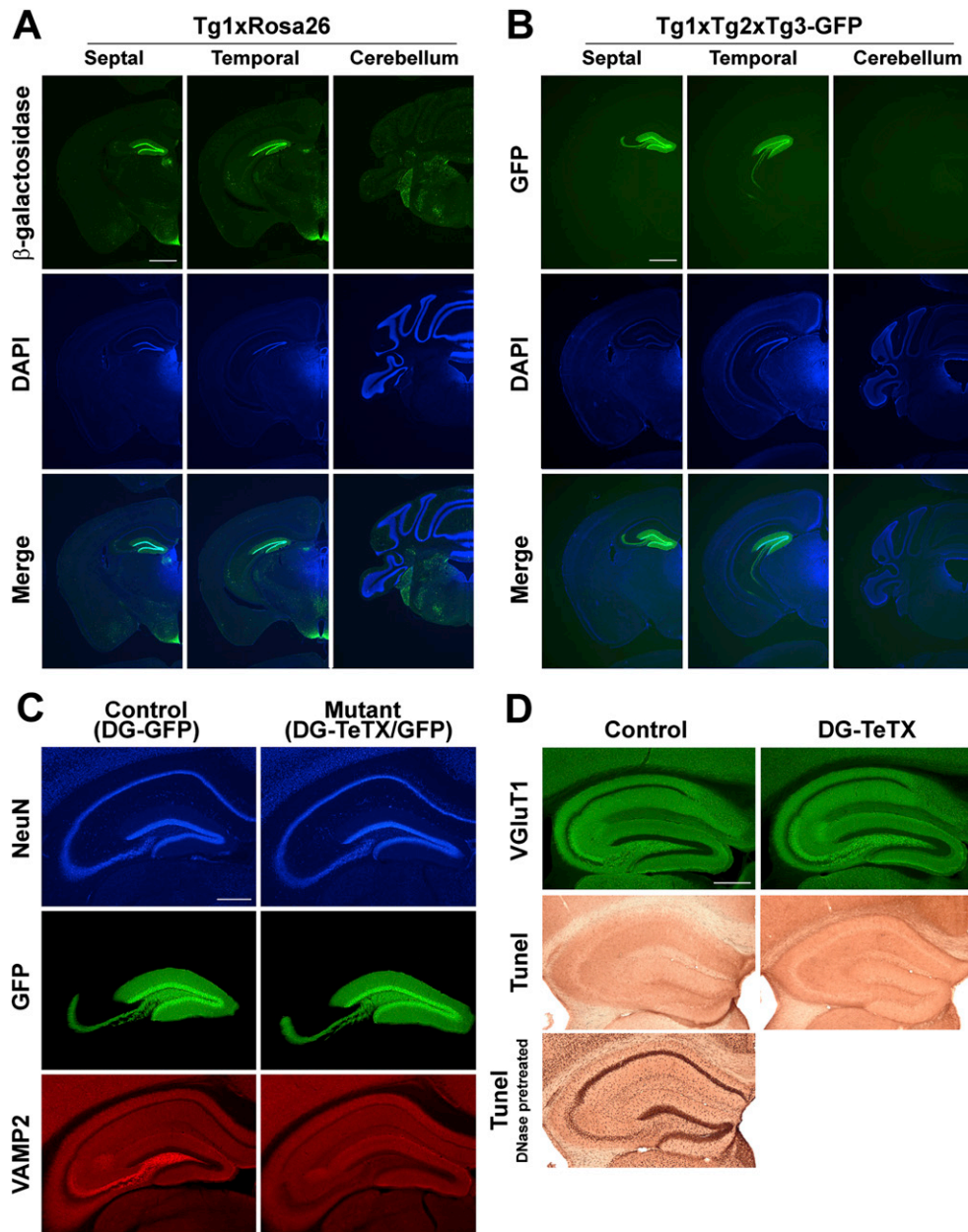


Figure S1. Greater Spatial Restriction of GFP Expression to the DG throughout the Septotemporal Axis with Two-Promoter Strategy and Additional Morphological Characterization of Activated DG-TeTX Mice, Related to Figure 1

(A and B) The two-promoter strategy robustly restricted GFP expression to the DG throughout the septotemporal axis. (A) Coronal sections from a 12-week-old Tg1xROSA26 mouse (single-promoter strategy) stained with an antibody specific for β -galactosidase (green) and cell nuclei marker, DAPI (blue). Merged images are for DAPI and β -galactosidase. β -galactosidase, an indicator for Cre-loxP recombination, was confined to cell somas and was robustly expressed in the DG as well as modestly in the arcuate nucleus of the hypothalamus and the lateral habenular nucleus. (B) Coronal sections of a 12-week-old DG-GFP mouse (Tg1xTg2xTg3-GFP, two-promoter strategy) raised on Dox and followed by a 2 week Dox withdrawal, stained with an antibody specific for GFP (green) and DAPI (blue). Merged images are for DAPI and GFP. GFP was detected in somas or in the axons and dendrites. However, in contrast to the β -galactosidase expression in the Tg1xROSA26 mouse, GFP expression in the DG-GFP mouse was highly restricted to the DG throughout the septotemporal axis.

(C and D) Lack of abnormalities in the hippocampal cytoarchitecture, MF projection and cell death in activated DG-TeTX mice. (C) Triple immunostaining of coronal sections from a 14-week-old activated DG-GFP control mouse and an activated quadruple Tg1xTg2xTg3-GFPxTg3-TeTX (DG-TeTX/GFP) mutant mouse stained with anti-NeuN (blue), anti-GFP (green) and anti-VAMP2 (red). (D) Hippocampal sections stained with an anti-VGLUT1 antibody (vesicular glutamate transporter 1, a presynaptic marker for glutamatergic nerve terminals) from 14-week-old control (Tg1xTg3-TeTX) and activated DG-TeTX mice, and hippocampal sections with TUNEL staining (a marker for cell death) from control and activated DG-TeTX mice. Bottom left, a positive control in which the section was treated with DNase I prior to TUNEL staining.

Scale bars in (A) and (B), 1 mm; (C) and (D), 500 μ m.

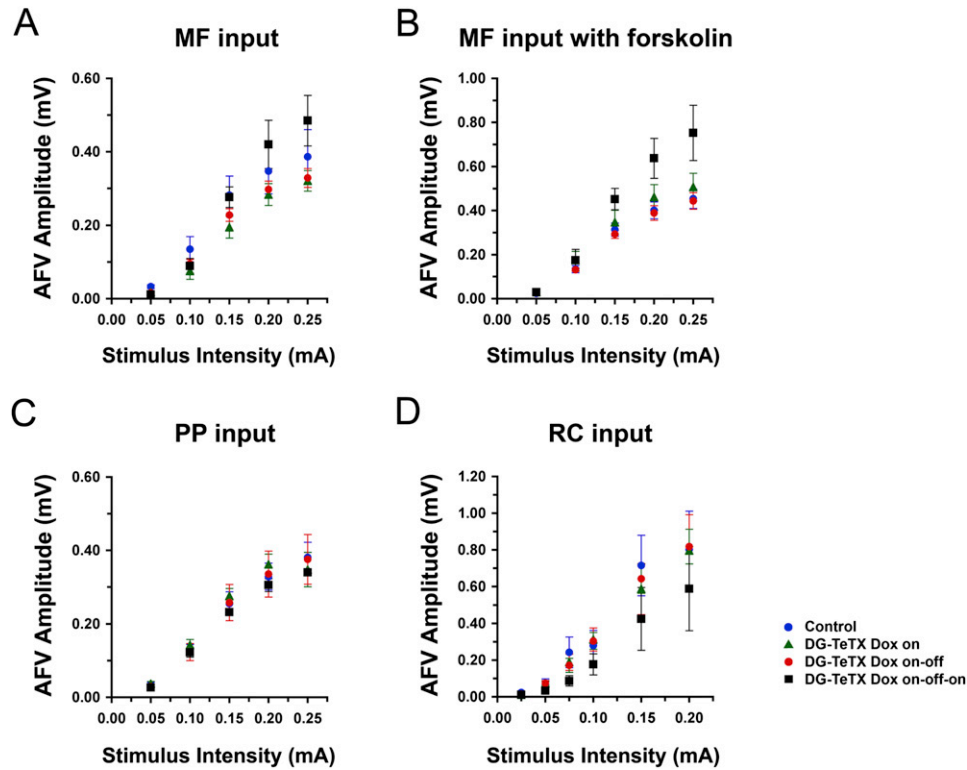


Figure S2. MF Excitability Is Normal in Activated DG-TeTX Mice, Related to Figure 2

(A and B) Afferent fiber volley (AFV) plotted as a function of stimulus strength for MF inputs in control ACSF (A) or in the presence of forskolin (B).

(C and D) Same as (A), but for PP inputs (C) and RC inputs (D). Blue circles, control littermates raised on Dox followed by a 6-week Dox withdrawal; green triangles, repressed DG-TeTX mice (always Dox-on); red circles, activated DG-TeTX mice (Dox-on-off) raised under the Dox-on condition followed by 6 week Dox withdrawal; black squares, re-repressed DG-TeTX (Dox-on-off-on) mice, which had been raised under the Dox-on condition and then underwent a 6 week Dox withdrawal, followed by a 4 week Dox readministration. Note that these curves were generated by analysis of recordings used to monitor fEPSP data presented in Figures 2A–2D. The lack of any significant difference across genotype/condition ($p > 0.05$, t test) indicates that the deficit in MF transmission of activated DG-TeTX mice (Figures 2A and 2B) is not due to a failure of action potential propagation through the MF pathway or the stimulation of fewer fibers.

Data represent mean \pm SEM.

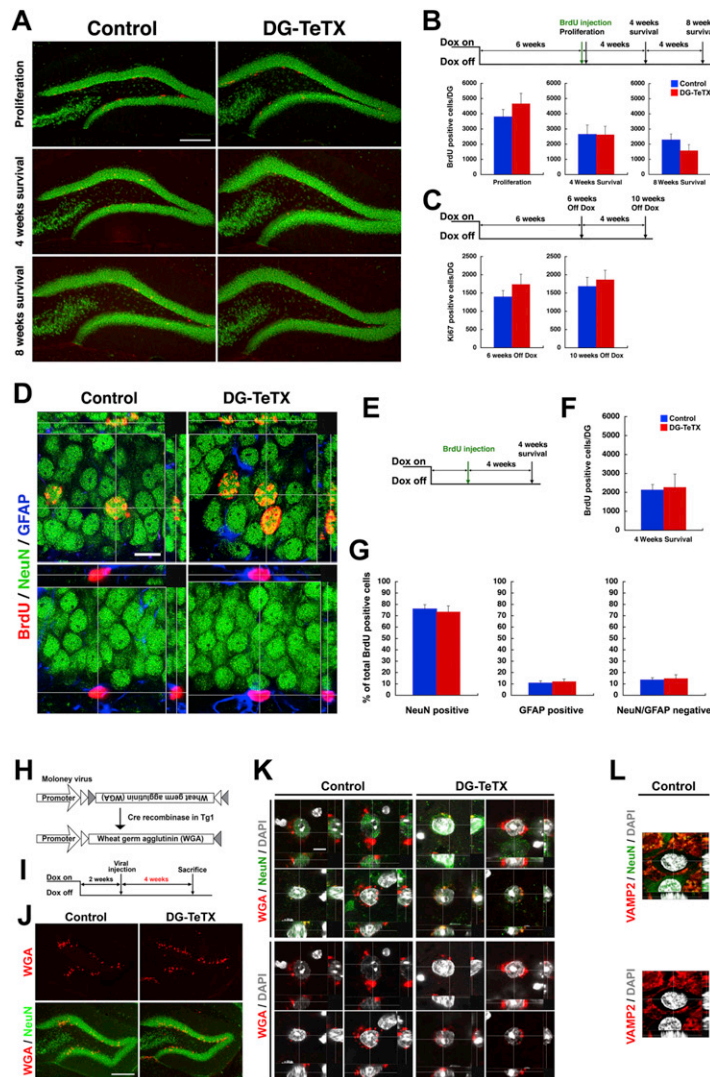


Figure S3. Normal Adult Neurogenesis and Integrity of MF Transmission from Young Adult-Born GCs in Activated DG-TeTX Mice, Related Figure 3

(A) Hippocampal sections stained with anti-BrdU (red) and anti-NeuN (green) from control and activated DG-TeTX mice 1 day (Proliferation), 4 weeks and 8 weeks following BrdU injection.

(B) Number of BrdU-positive cells in the DG.

(C) Number of Ki67-positive cells (a marker for proliferating cells) in the DG. Dox and BrdU injection schedules are above each panel. There was no difference between the two genotypes in the numbers of BrdU- and Ki67-positive cells ($p > 0.05$ for each condition, t test).

(D) Confocal images at a single z axis with red for BrdU, green for NeuN, and blue for GFAP. Optical sections along the horizontal or vertical lines across multiple z axes are shown on the top and right, respectively.

(E) Dox and BrdU injection schedules for experiments in (F) and (G).

(F) Numbers of BrdU-positive cells in the DG.

(G) Proportion of NeuN-positive, GFAP-positive, and NeuN/GFAP-negative cells among BrdU-positive cells. There was no significant genotype-specific differences in the number of BrdU-positive cells, in the proportion of NeuN-positive, GFAP-positive cells or in the proportion of NeuN/GFP-negative cells among the BrdU-positive cells ($p > 0.05$ for each cell type, t test).

(H) A Moloney viral vector encoding Cre/loxP-dependent WGA. A Cre-loxP recombination occurring between 1 and 2 weeks after viral injection (Figure S4).

(I) Dox diet and viral injection schedules.

(J) DG areas of sections stained with anti-WGA (red) and costained with anti-NeuN (green) from control and activated DG-TeTX mice.

(K) Confocal images of representative neurons from the hilar regions of control and activated DG-TeTX mice. Neurons (top) colored with red (WGA), green (NeuN), and gray (DAPI). The same neurons (bottom) colored with red (WGA) and gray (DAPI). Note that WGA is localized immediately adjacent to DAPI-stained nuclei. (L) All presynaptic terminals labeled with anti-VAMP2 (red) remained at some distance away from DAPI-positive nuclei, whereas WGA signals in (K) were in close proximity of DAPI-positive nuclei, suggesting that the WGA observed in (K) is not at the presynaptic terminals but has crossed synapses and has accumulated in postsynaptic cells, perhaps associated with the endoplasmic reticulum.

Scale bars in (A), 250 μm ; (D), 10 μm ; (J), 250 μm ; (K), 5 μm . Data represent mean \pm SEM.

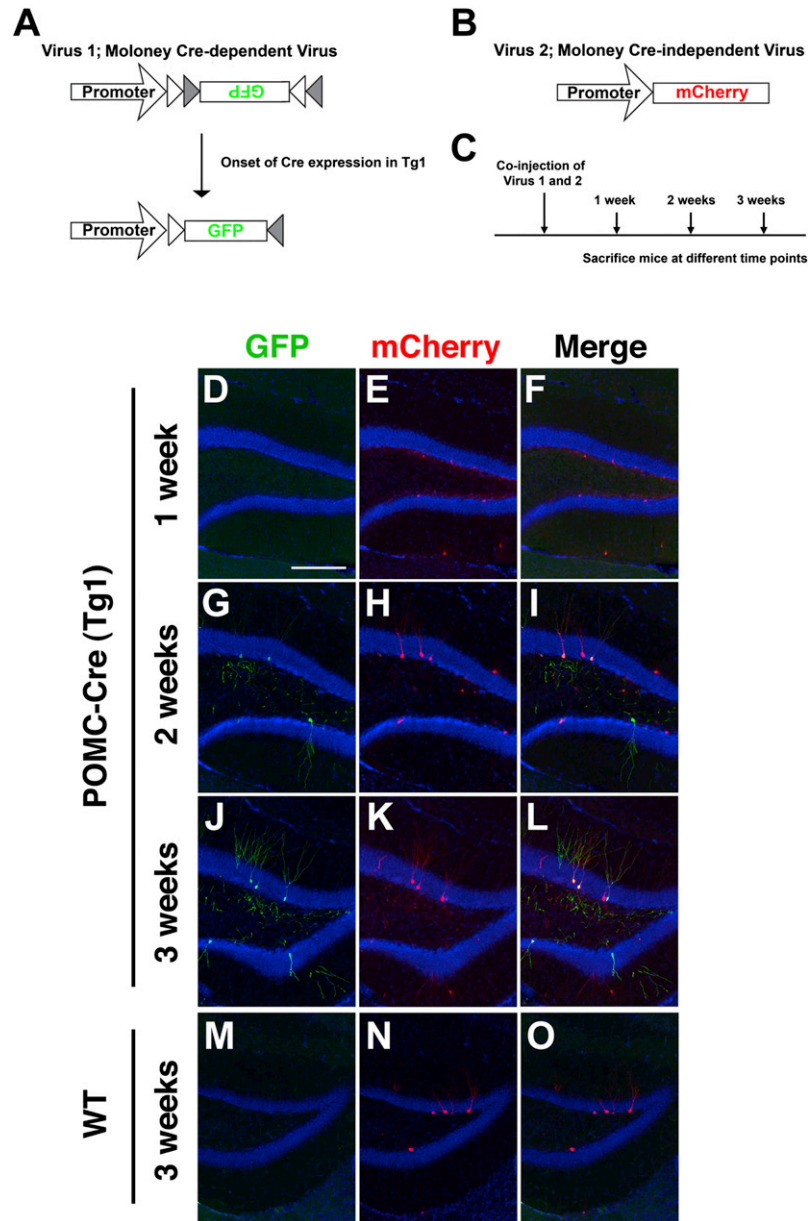


Figure S4. Time Course of Cre-loxP Recombination along the Maturation of Adult-Born GCs in POMC-Cre (Tg1) Mice, Related to Figures 4 and S3

(A) A Cre-dependent Moloney viral vector (virus 1) encoding GFP.

(B) A Cre-independent Moloney viral vector (virus 2) encoding mCherry to assess successful virus injection.

(C) A schedule of analysis relative to the viral injection.

(D–L) Images of the DG from POMC-Cre (Tg1) mice in which viruses 1 and 2 were co-injected into the DG at 1 week (D–F), 2 weeks (G–I), and 3 weeks (J–L) prior to analyses. Hippocampal sections were stained with anti-GFP (green; D, G, and J) and anti-mCherry (red; E, H, and K). (F, I, and L) Merged images.

(M–O) Images of the DG from a wild-type mouse co-injected with viruses 1 and 2 into the DG at 3 weeks prior to analyses. The blue color is for DAPI (D–O). Note that GFP signals were first detected at 2 weeks after viral injection (G). mCherry signals were detected at all time points in Tg1 and wild-type mice, but no GFP signal was observed in the wild-type mouse or in the Tg1 mouse at 1 week after viral injection, indicating that Cre-loxP recombination occurred in the adult-born DG GCs between 1 and 2 weeks of cellular age.

Scale bars (D)–(O), 250 μ m

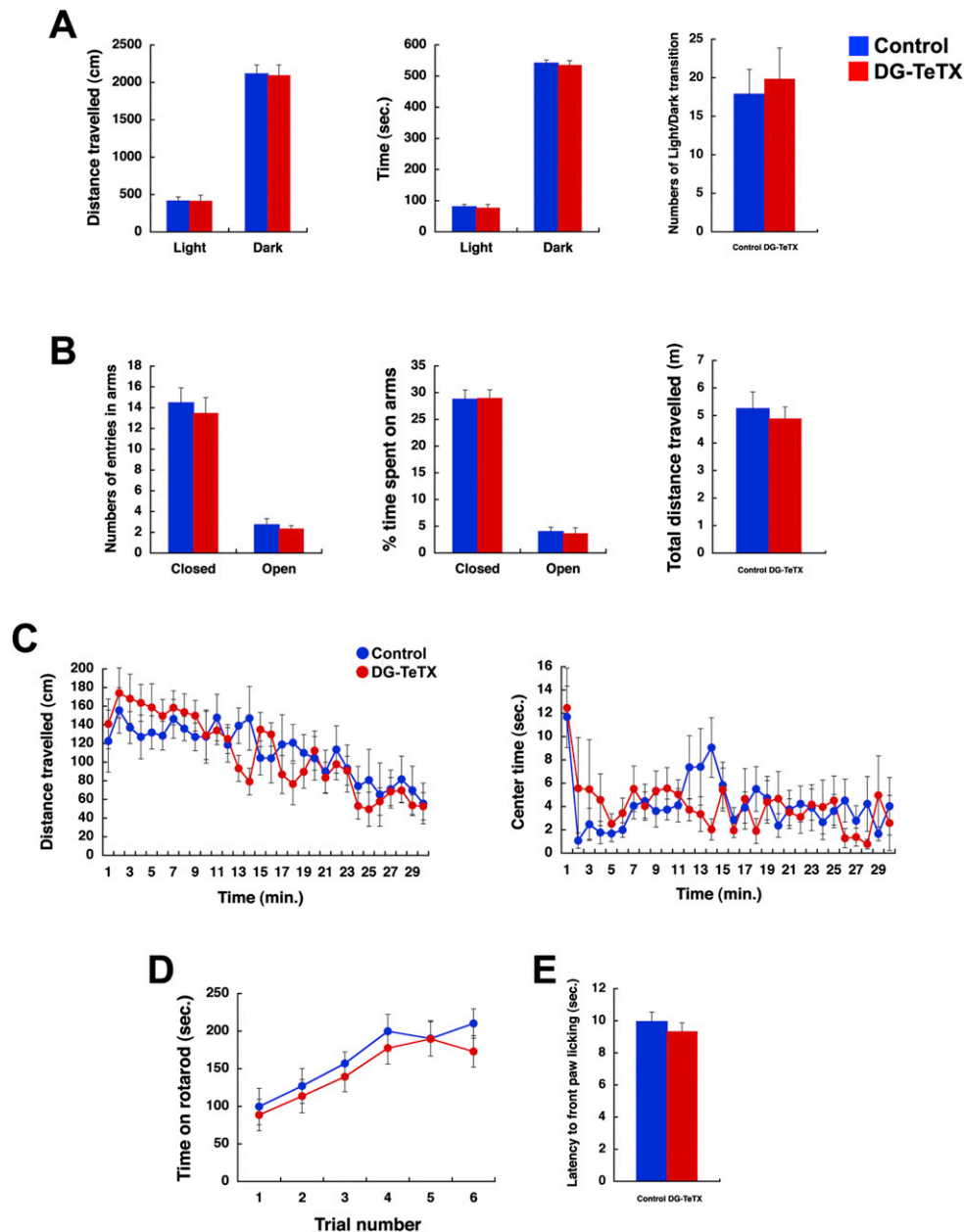


Figure S5. Activated DG-TeTX Mice Exhibited No Change in the Light/Dark Transition, Elevated Plus Maze, Open Field, Rotarod, and Hot Plate Tests, Related to Figure 5

(A) Performance in the light/dark transition test of activated DG-TeTX mice (red) and their control littermates (blue). There was no significant difference between the two genotypes in the distance traveled in each compartment ($p > 0.05$ for both light and dark compartments, t test), in the total time spent in each compartment ($p > 0.05$ for both light and dark compartments, t test) or in the number of transitions between the light and dark compartments ($p > 0.05$, t test; $n = 12$ per genotype).

(B) Performance in the elevated plus maze test. No significant difference was observed between the two genotypes in the number of entries into each arm ($p > 0.05$ for both closed and open arms, t test), in the percentages of time spent in each arm ($p > 0.05$ for both closed and open arms, t test) or in the total distance traveled on the maze ($p > 0.05$, t test; $n = 12$ per genotype).

(C) Performance in the open field test for a 30 min session in a novel chamber. There was no significant difference between the two genotypes in the total distance traveled (ANOVA, genotype: $F_{(1,22)} = 0.013$, $p = 0.912$) or in the time spent at the arena center (ANOVA, genotype: $F_{(1,22)} = 0.007$, $p = 0.932$; $n = 12$ per genotype).

(D) Performance in the rotarod test along six trials of activated DG-TeTX mice ($n = 15$) and their control littermates ($n = 13$). No significant difference was detected between the two genotypes (ANOVA, genotype: $F_{(1, 26)} = 0.440$, $p = 0.513$).

(E) Performance in the hot plate test. There was no significant difference between genotypes in the latency to lift the front paws ($p > 0.05$, t test; $n = 12$ per genotype).

Data represent mean \pm SEM.

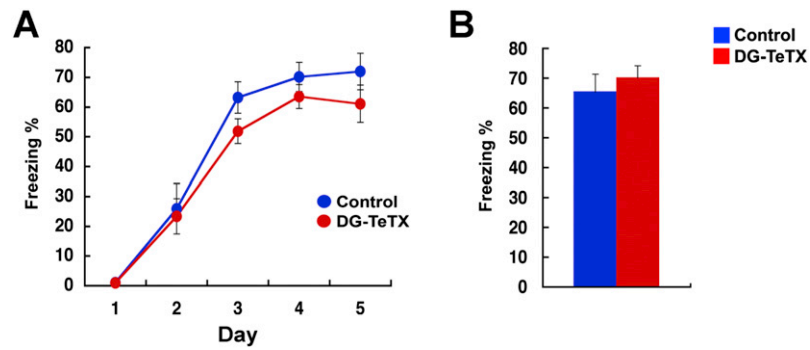


Figure S6. Contextual Fear Memory Acquired during Dox-on Condition Does Not Decay during a Subsequent 4 Week-Long Dox-off Treatment in DG-TeTX Mice, Related to Figure 7

(A) Freezing of DG-TeTX mice and their control littermates ($n = 12$ per genotype) during the 5 days of fear conditioning under the Dox-on condition (CS; 3 min contextual exposure per day, US; a single footshock per day for 2 s, 0.65 mA). No difference was observed in freezing levels between genotypes during the 5 days of fear conditioning (ANOVA, genotype: $F_{(1,22)} = 1.725$, $p = 0.203$).

(B) The conditioned mice were kept in their home cages for 4 weeks under the Dox-off condition and then subjected to context-dependent memory recall by being returned to the original context (no shock) for 3 min while freezing was scored. There was no difference in freezing levels between genotypes ($p > 0.05$, t test). Data represent mean \pm SEM.

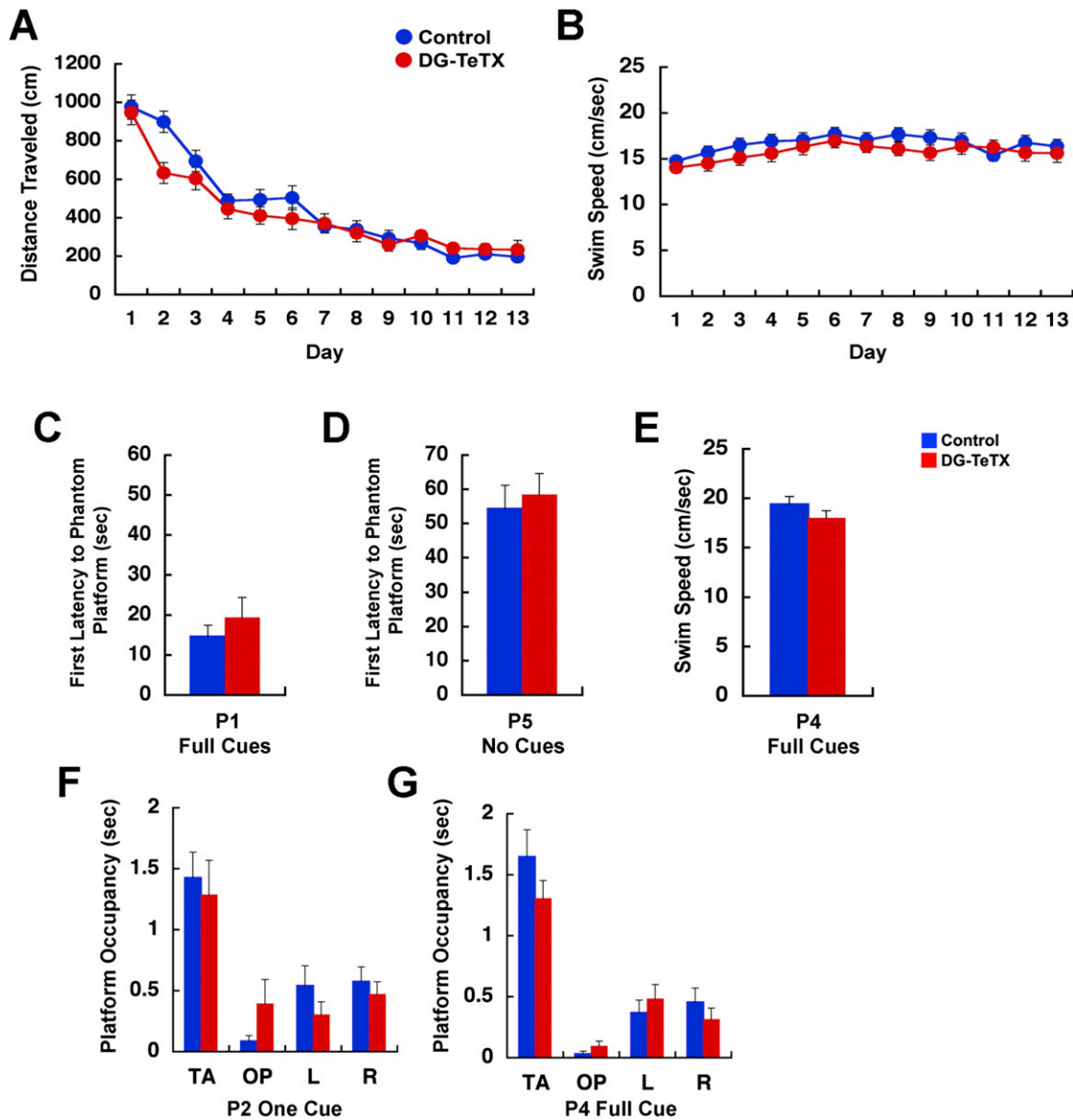


Figure S7. Additional Data for the Spatial Pattern Completion Experiment, Related to Figure 7

(A and B) During the Morris water maze training of repressed (i.e., Dox-on) DG-TeTX mice ($n = 23$) and their control littermates ($n = 24$), there was no genotype-specific difference in the total distance traveled to reach the hidden platform (A, ANOVA, genotype: $F_{(1,45)} = 1.806$, $p = 0.186$) or in the swim speed (B, ANOVA, genotype: $F_{(1,45)} = 1.450$, $p = 0.235$).

(C and D) Latency for the first crossing of the phantom platform during the probe trial with the full set of cues (P1, C, $p > 0.05$ between genotypes, t test) or no cue (P5, D, $p > 0.05$ between genotypes, t test).

(E) No genotype-specific difference in swim speed during the probe trial with the full set of cues (P4, $p > 0.05$, t test).

(F and G) The amount of time (s) the mice spent during the 90 s-long probe trial under one (F, P2) and the full set of cues (G, P4) in the circular (diameter 13 cm) platform location in the target quadrant (TA) and the corresponding locations in each of the other three quadrants (OP, opposite; L, left; R, right). No genotype-specific difference with either one cue or four (i.e., a full set of) cues (ANOVA in TA of P2 and P4, genotype \times cue: $F_{(1,45)} = 0.321$, $p = 0.574$; genotype: $F_{(1,45)} = 0.947$, $p = 0.336$; cue: $F_{(1,45)} = 0.457$, $p = 0.503$).

Data represent mean \pm SEM.